

Reducing Bias in Cropland Soil Organic Carbon and Clay Predictions using Sentinel-2 Composites and Data Balancing

Tom Broeg^{a,c*}, Axel Don^b, Thomas Scholten^c, Stefan Erasmi^a

^aThünen Earth Observation (ThEO), Thünen Institute of Farm Economics, Bundesallee 63, 38116 Braunschweig, Germany

^bThünen Institute of Climate-Smart Agriculture, Bundesallee, 65, 38116 Braunschweig, Germany

^cDepartment of Geosciences, Soil Science and Geomorphology, University of Tübingen, 72070 Tübingen, Germany

*Correspondence: tom.broeg@thuenen.de

VI: Submitted to Remote Sensing of Environment on May 09th, 2025

Non-peer-reviewed preprint submitted to EarthArXiv on May 14th, 2025

Abstract

Accurate maps of cropland soil organic carbon stocks (SOCS) and clay content are essential for climate-smart agriculture. Soil reflectance composites (SRC), derived from multispectral bare soil observations, offer a scalable approach to high-resolution soil mapping. While studies often focus on maximizing model performance, challenges remain regarding (1) the bias introduced by masking and excluding soil samples during SRC generation and (2) the accurate representation of the full range and distribution of soil properties in the resulting maps. Evaluating different SRC parameters, we found that commonly used indices such as the Normalized Burn Ratio 2 (NBR2) and the Normalized Difference Vegetation Index (NDVI) were significantly correlated with clay content and SOCS, respectively. These dependencies can lead to the systematic exclusion of high SOCS (>80 Mg ha⁻¹) and clay (>30 mass%) samples during SRC generation, introducing bias in the resulting maps. Models trained solely on SRC bands failed to capture the full range of the training data, limiting the applicability of the soil property maps. While the inclusion of additional remote sensing features, such as spectral-temporal metrics and indices, significantly improved the prediction accuracy, the representation of the imbalanced samples remained challenging. We demonstrated that a combined framework of spatial data augmentation and majority undersampling was effective in improving the range and concordance correlation coefficient (CCC) of the

predictions (SOCS = 0.82; Clay = 0.9). Our findings emphasize the importance of (1) evaluating excluded samples to identify potential SRC-induced bias, and (2) optimizing model predictions reflecting the observed data range to improve the reliability and usability of the resulting soil maps.

Keywords

Soil Reflectance Composite, Bare Soil Mosaic, Digital Soil Mapping, Imbalanced Regression, Soil Organic Carbon Stocks, Clay Content, Cropland

Highlights

- Soil indices can introduce bias in soil reflectance composites for cropland mapping
- NDVI and NBR2 exclude high SOCS/clay samples, reducing map accuracy and usability
- Baseline models underpredict high values and fail to capture sample distributions
- Data balancing improves prediction range and CCC (SOCS = 0.82; Clay = 0.90)
- Assessing excluded samples and prediction bias improves soil map reliability

1 Introduction

It is estimated that due to land use change and cropland intensification, most agricultural soils have lost up to 50 % of their original carbon stocks, significantly contributing to climate change (Lal, 2003). As the largest terrestrial C pool, soil organic carbon (SOC) is a central aspect of European policies like the Green Deal, targeting to achieve climate neutrality by 2050 (Montanarella & Panagos, 2021). The sequestration of atmospheric CO₂ in agricultural soils, promoted by initiatives such as ‘4 per 1000’, is widely recognized as a win-win strategy to both mitigate climate change and improve soil health (Minasny et al., 2017). Most of the SOC stock (SOCS) is concentrated in the topsoil (0–30 cm) and is essential for soil functions, including erosion control, nutrient cycling, water retention, and aggregate stabilization (Murphy, 2015). As a key component of the global carbon cycle, SOCS are dynamic and vary spatially and temporally due to agricultural management practices (e.g., fertilization, tillage, intensification) and site-specific biophysical factors such as climate and soil properties (Wiesmeier et al., 2019). Clay minerals play a crucial role in carbon retention due to their high sorption rates and ability to stabilize SOC in soil aggregates, making the clay content a key factor in predicting and interpreting SOCS (Prout et al., 2021; Rasmussen et al., 2018).

The demand for spatially explicit information on biogeochemical and physical soil properties has grown significantly in recent decades (Paustian et al., 2019). National soil sampling campaigns, such as the German Agricultural Soil Inventory (BZE-LW), can provide such soil data but are time-consuming and limited in sample size (Poeplau, Jacobs, et al., 2020). Based on soil measurements, it has been shown that the SOCS can vary significantly across regional, local, and plot scales, further increasing the need for high-resolution soil data (Don et al., 2007; Poeplau et al., 2022). To address this issue, various digital soil mapping (DSM) frameworks have been developed to predict soil properties at different levels (Chen et al., 2022). Earth observation (EO) can play a crucial role in improving the accuracy, resolution, and transferability of predicted maps (Broeg et al., 2023; Tziolas et al., 2021). Recent works highlight the potential of soil reflectance composites (SRC), derived from multispectral bare soil observations, to directly analyze cropland soil properties through spectral responses (Broeg et al., 2024; Demattê et al., 2018; Diek et al., 2017; Rogge et al., 2018). With the growing number of studies, however, questions arise on what factors should be considered when optimizing and comparing different SRC frameworks for the prediction of reliable and unbiased soil maps (Vaudour et al., 2022).

Most soil reflectance composite (SRC) workflows use spectral indices to determine whether a pixel represents bare soil or is influenced by vegetation or other surface covers (Delaney et al., 2025). In general, the selection of optimal indices and thresholding values serves two key purposes. First, pixels and samples without valid bare soil observations are masked out and excluded from the soil map. Second, the highest-quality bare soil observations are selected to enhance the soil signal and improve the model accuracy (Dvorakova et al., 2022). Studies have shown that methods of soil spectroscopy can be applied to optimize and refine the SRC parameter settings (Dvorakova et al., 2020; Heiden et al., 2022). Demattê et al. (2018) demonstrated that under laboratory conditions, the Normalized Difference Vegetation Index (NDVI) increases incrementally when adding photosynthetic vegetation, and recommended a threshold of 0.25 to select bare soil pixels. Other studies based on spectral soil libraries indicate, however, that the NDVI is not only influenced by the presence of vegetation but also by the soil itself (Montandon & Small, 2008). As a result, NDVI thresholds of 0.35 and higher have been recommended to account for a broader range of bare soil conditions (Broeg et al., 2024; Safanelli et al., 2020). While many studies focus on maximizing the spectral quality of the soil signal, less is known about the interactions between bare soil indices and

soil properties and the potential influence on the exclusion of specific soil conditions during SRC generation.

In addition to laboratory analyses, efforts have been made to evaluate and compare SRC parameters based on the performance of the final soil models. It has been suggested that predictive power can serve as a proxy for spectral quality, as it reflects the selection of the purest bare soil observations for the SRC (Dvorakova et al., 2021). Multiple studies have highlighted the significant influence of the Normalized Burn Ratio 2 (NBR2), derived from shortwave infrared (SWIR) bands, on the SOC prediction accuracy (Gomez et al., 2022; Vaudour et al., 2021). Low NBR2 values are associated with optimal seedbed conditions, characterized by dry, homogenized soils that are free from vegetation and residues (Dvorakova et al., 2022). Further research has shown, however, that NBR2 can also be affected by the soil clay content, complicating its interpretation (Shabou et al., 2015). While the most accurate SOC models are typically achieved using very low NBR2 thresholds (<0.08), values up to 0.15 are often required to capture a broader range of bare soil conditions (Demattê et al., 2018; Safanelli et al., 2020). In many cases, this trade-off has been resolved by prioritizing prediction accuracy over spatial coverage, significantly reducing the number of soil samples available for modeling (Castaldi et al., 2019; Demattê et al., 2018; Dvorakova et al., 2022; Silvero et al., 2021; Vaudour et al., 2021). Considering these interdependencies, questions remain about whether the selection of bare soil indices and thresholds affects the exclusion of certain soil parameters (e.g., the clay content) from the soil models, influencing the bias and applicability of the final maps.

Another key challenge in DSM is the accurate representation of soil properties with skewed distributions, such as the SOC, which often includes outliers and extreme values that are underrepresented in the training data. Studies have shown that in this case, models tend to underpredict high values and fail to reproduce the SOC range of the samples (De Brogniez et al., 2015; Rawlins et al., 2009). Feeney et al. (2022) argue that the availability and quality of environmental covariates are major factors limiting model performance and the accurate representation of extreme values. Zepp et al. (2021) showed that the calculation of additional spectral indices, based on the original SRC bands, improved model accuracy but did not affect the range of predicted SOC values. Other studies reported that including further EO-based covariates such as spectral temporal metrics (STM) (Stumpf et al., 2024) or digital elevation models (DEM) (Žižala et al., 2022) can improve the overall model performance, though at an increased risk of

overfitting (Meyer et al., 2019). It has been shown that in classification tasks, such as the predictions of soil types, DSM models tend to minimize uncertainty by favoring majority classes (Rau et al., 2024). While issues regarding class imbalance have been successfully addressed using over- and undersampling (Sharififar et al., 2019), it remains unclear whether similar methods can improve the predictions of continuous variables like SOCS and clay content.

In this study, we present a novel framework to evaluate and compare different Sentinel-2 SRC for producing large-scale soil property maps. Based on high-quality SOCS and clay content samples from the German Agricultural Soil Inventory, we assessed the predictive power of each SRC using band-wise regressions and support vector machines (SVM). Rather than only considering soil samples that are covered by the SRC, we quantified potential mapping bias by comparing the SOCS and clay values between samples that have been included and excluded/masked out from the soil maps. To evaluate the reliability of the resulting predictions, we further analyzed the extent to which the models reproduced the full range and distribution of measured soil properties. In summary, the following three research questions were addressed:

- How does the predictive power of the SRC for mapping SOCS and clay depend on the choice of bare soil indices and thresholding values?
- How do interactions between the bare soil indices and soil properties influence the exclusion of soil samples and the potential introduction of bias during SRC generation?
- To what extent is it possible to further improve the distribution and range of SOCS and clay predictions using additional EO features and data balancing methods?

2 Material and Methods

2.1 Research Area

Germany covers a land area of 357,592 km², with roughly 36% dedicated to cropland (Destatis, 2022). The soil conditions are diverse and can be divided into seven major landscape regions that follow a general North-South gradient: the Northern Plain, Loess Hills, Eastern and Western Highlands, Southern Scarplands, Alpine Foreland, and the Alps (Fig. 1). The North German Plain was formed by glacial processes and is mostly flat with sandy soils. In the northwestern part of the plain, organic soils are common in lowlands and are often drained for agricultural purposes. The

Loess Hills in Central East Germany are covered by aeolian sediments, resulting in the presence of fertile loamy soils. The Eastern and Western Highlands feature multiple low mountain ranges below 1,500 m a.s.l. with diverse soils depending on various bedrocks. In the South German Scarplands, changing sediments from the Devonian and Triassic induced the formation of diverse textures, including clay-rich soils. The Alpine Foreland is influenced by glaciofluvial deposits from the Tertiary Molasse Basin and primarily consists of loamy soils. Organic soils are found in the pre-Alpine lowlands that are fed by mountain rivers. Towards the Alps in the south, the altitude increases, and cropland areas decrease and are substituted by grassland.

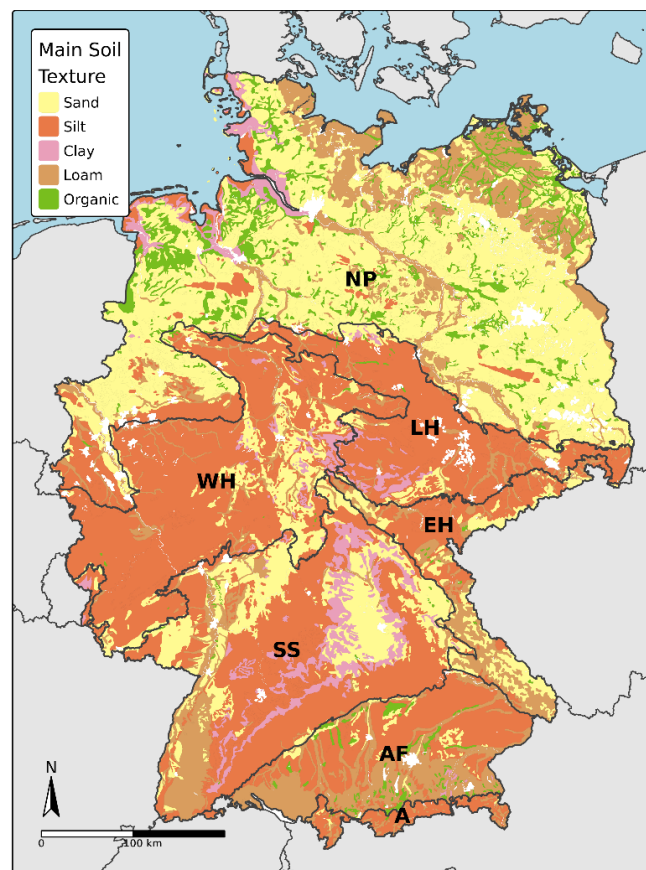


Figure 1: Overview of the research area. Main soil texture (BGR, 2007) and major landscape regions in Germany (Thünnen-Institut, 2022). NP = Northern Plain; LH = Loess Hills; WH = Western Highlands; EH = Eastern Highlands; SS = Southern Scarplands; AF = Alpine Foreland; A = Alps. Map lines delineate study areas and do not necessarily depict accepted national boundaries.

2.2 Soil Samples

The soil samples in this study were collected as part of the first German Agricultural Soil Inventory (BZE-LW), conducted from 2011 to 2018 (Poeplau, Don, et al., 2020). A total of 2,254 cropland soils were sampled based on an 8 × 8 km regular grid across Germany (Fig. 2). At each site, a one-meter soil profile was excavated and a composite sample (around 1 kg) was collected from five fixed depth increments for chemical and textural analysis: 0–10 cm, 10–30 cm, 30–50 cm, 50–70 cm, and 70–100 cm. Additionally, two to ten undisturbed samples were taken to determine the bulk density and rock fragment fraction. The SOCS were estimated according to methods described by Poeplau et al. (2017). First, the composite samples were oven-dried at 40 °C and sieved to 2 mm to determine the SOC content of the fine soil using dry combustion. Next, the fine soil stocks (FSS in Mg ha⁻¹) were estimated for each depth increment (*i*) using the undisturbed samples

$$FSS_i = \frac{mass_{fine\ soil}}{volume_{sample}} \times depth_i, \quad (1)$$

and the SOCS (Mg ha⁻¹) were calculated using

$$SOCS_i = SOC_{fine\ soil} \times FSS_i. \quad (2)$$

To determine the total topsoil SOCS of each cropland site in 0–30 cm, the measurements of the depth increments 0–10 and 10–20 cm were combined. The clay content (mass%) of the fine soil was determined for each depth increment using sieving and sedimentation techniques, based on the dried composite samples. The total clay content of the topsoil (0–30 cm) was estimated using a weighted average of the depth increments 0–10 and 10–20 cm. An overview of the measured SOCS and clay distributions is given in Fig. 2.

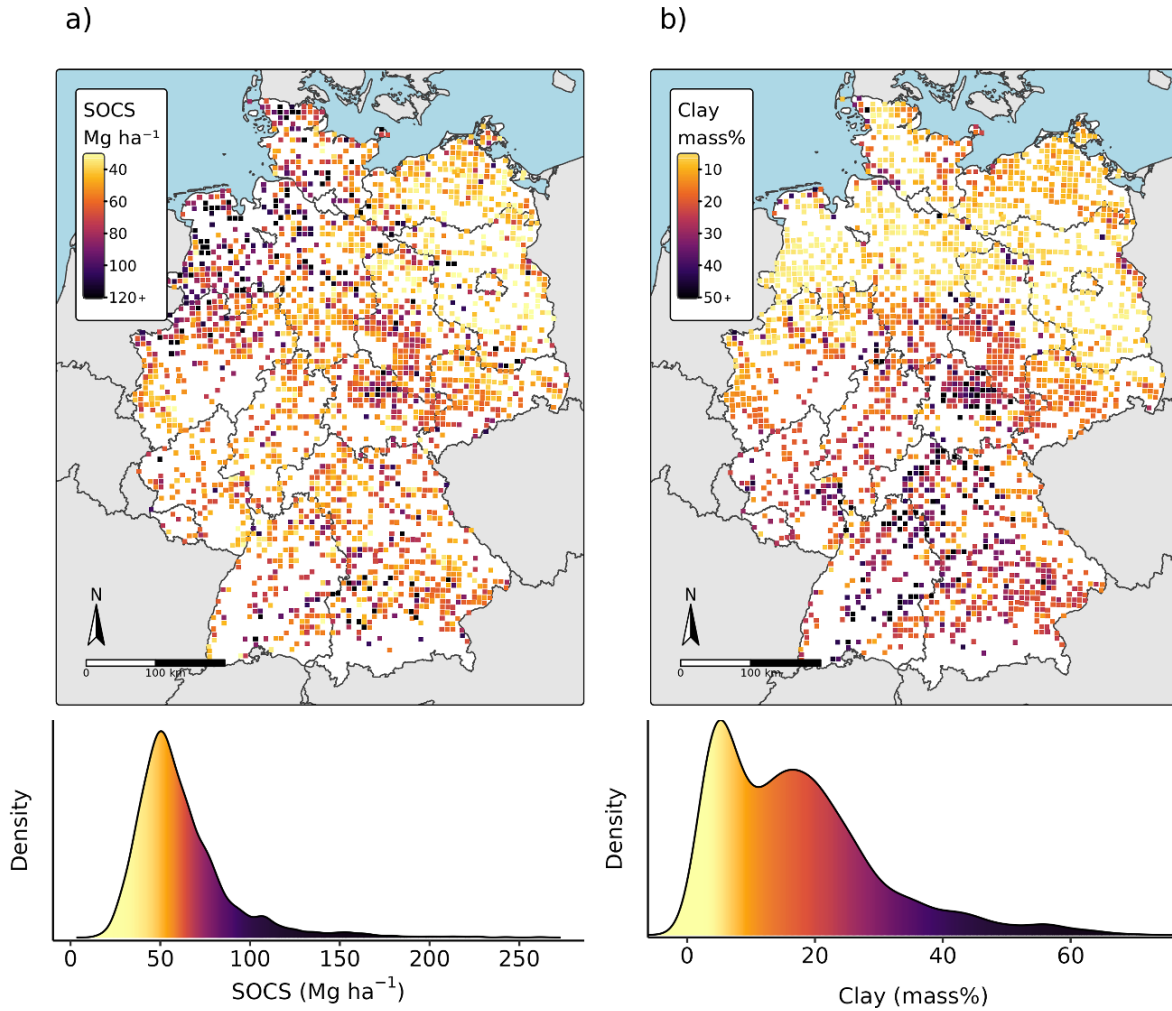


Figure 2: Overview of the cropland sampling locations and the distributions of the measured SOCS (a) and clay content (b) in Germany.

2.3 Sentinel-2 Data Preparation

The remote sensing data used in this study was processed and organized using the Framework for Operational Radiometric Correction for Environmental Monitoring (FORCE) (Frantz, 2019). All available Sentinel-2A/B scenes from February to November (2015–2024) were collected and organized into a data cube using the FORCE level-1 module. The scenes from December and January were excluded to minimize interference from snow cover and water logging, which can lead to a distortion of the soil signal. To prepare an analysis-ready data cube, the data was preprocessed with the FORCE level-2 module, including cloud masking, radiometric corrections, co-registration, and resolution merging (Frantz, 2019).

Cloud and cloud shadow detections were carried out using a modified version of the Fmask algorithm (Frantz et al., 2015; Zhu & Woodcock, 2012). Based on parallax effects between the Sentinel-2 near-infrared bands, a cloud displacement index was implemented to distinguish clouds from land features (Frantz et al., 2018). A 300 m buffer was applied around clouds to remove hazy transition zones, and pixels identified as opaque clouds were marked out to prevent spectral distortions unrelated to the land surface. All Sentinel-2 scenes with an estimated cloud cover below 70 % were considered for the data cube.

Radiometric corrections were used to convert the top-of-atmosphere reflectance through radiative transfer modeling, as described in Frantz et al. (2016). Adjustments were used to account for atmospheric conditions like aerosol optical depth and water vapor, using the 1 arc-second Copernicus Digital Elevation Model for accurate path length corrections. Additionally, corrections for adjacency effects, bidirectional reflectance distribution function (BRDF), and topography were applied. An enhanced C-correction method was used to reduce illumination artifacts in sloped areas (Buchner et al., 2020).

To address geolocation errors in the pre-Global Reference Image (GRI) Sentinel-2 data, the scenes were co-registered with Landsat base images to improve geometric accuracy (Rufin et al., 2021). A data fusion algorithm (ImproPhe) was applied to increase the spatial resolution of the 20-meter Sentinel-2 bands (5, 6, 7, 8a, 11, 12) to a common resolution of 10 meters (Frantz, Stellmes, et al., 2016). The processed data was projected to the ETRS89-LAEA coordinate system (EPSG:3035) and used for the generation of the SRC in the following steps.

2.4 Soil Reflectance Composites

2.4.1 Bare Soil Indices and Thresholds

Using the preprocessed Sentinel-2 data cube, band-wise spectral averages of all available bare soil observations were calculated and used as primary model features for soil mapping. Four SRC variants were generated based on different combinations of bare soil indices (Table 1) and thresholding values (Table 2). Due to various effects (fallow land, land-use change, mixed pixels, etc.), it is expected that the SRC will be unable to cover all 2,234 soil samples. To ensure comparability of the results, the indices and thresholds were defined to cover a similar proportion of around 90% of the total soil samples (Table 2).

The NDVI and NBR2 are the most used bare soil indices with recommended thresholding values typically ranging from 0.25 to 0.35 (NDVI) and 0.05 to 0.16 (NBR2) (Delaney et al., 2025). Three combinations were tested to evaluate how lowering both thresholds (SRC1: Low NDVI, NBR2) or only one of them (SRC2: Low NDVI; SRC3: Low NBR2) affects the resulting SRC (Table 2). Thresholds with NBR2 values below 0.1 were avoided, as they would significantly reduce the spatial coverage of the SRC. An additional SRC was tested using a modified vegetation index (PV+IR2), proposed by Heiden et al. (2022) (Table 1). The corresponding threshold values (SRC4: Low PV+IR2) were selected to maintain a comparable number of training samples (~2000) across the four SRC variants (Table 2).

Table 1: Overview of the bare soil indices considered in this study (band names refer to Sentinel-2).

Index	Abb.	Equation	Source
Normalized Difference Vegetation Index	NDVI	$\frac{\overline{B8_{soil}} - \overline{B4_{soil}}}{\overline{B8_{soil}} + \overline{B4_{soil}}}$	Tucker (1979)
Normalized Burned Ratio 2	NBR2	$\frac{\overline{B11_{soil}} - \overline{B12_{soil}}}{\overline{B11_{soil}} + \overline{B12_{soil}}}$	Van Deventer et al. (1997)
Combined NDVI and SWIR2 index	PV+IR2	$\frac{\overline{B8_{soil}} - \overline{B4_{soil}}}{\overline{B8_{soil}} + \overline{B4_{soil}}} + \frac{\overline{B8_{soil}} - \overline{B12_{soil}}}{\overline{B8_{soil}} + \overline{B12_{soil}}}$	Heiden et al. (2022)

Table 2: Overview of the four SRC variants, derived in this study.

SRC No.	Name	Threshold 1	Threshold 2	Included samples (% from total)
1	Low NBR2, NDVI	NBR2 < 0.1	NDVI < 0.25	2003 (90)
2	Low NDVI	NBR2 < 0.16	NDVI < 0.25	2025 (91)
3	Low NBR2	NBR2 < 0.1	NDVI < 0.35	2028 (91)
4	Low PV+IR2	NBR2 < 0.16	PV+IR2 < 0.24	2038 (91)

2.4.2 Evaluation and Comparison of the SRC

The evaluation of the resulting SRC was conducted in multiple steps to assess (1) the predictive power of individual spectral bands for modeling cropland SOCS and clay content in Germany; and (2) the potential introduction of model bias due to the selective masking of specific soil samples. In the first step, linear regressions and R^2 values were derived for the ten SRC bands and the respective SOCS and clay samples. Next, support vector machines (SVM) (Cortes & Vapnik, 1995) were used to model both soil properties using all SRC bands as input features. For the SVM, a radial kernel was applied with default settings (epsilon = 0.1; cost = 1) without additional parameter tuning.

Since the SRC were designed to cover roughly the same proportion of total soil measurements, we were able to compare the potential bias introduced by selective sample masking. To quantify the results, we analyzed how closely the probability distributions of included ($\approx 90\%$) and excluded ($\approx 10\%$) soil samples aligned for each SRC using the Wasserstein distance (W_p) (Vaserstein, 1969). The W_p evaluates the costs of converting one distribution into another one, providing an estimation of the model bias that is introduced by excluding certain soil properties. To simplify the comparison of the SOCS and clay, the W_p values were normalized by dividing them by the standard deviation of the corresponding soil property. To further examine relationships between the bare soil indices and soil samples included in the four SRC, scatter plots with linear regressions were plotted for NDVI, NBR2, and PV+IR2, and the corresponding SOCS and clay measurements.

2.5 Additional Covariates and Feature Importance

To assess whether the model performance could be further improved, we tested the inclusion of additional EO-based features alongside the ten original Sentinel-2 bands (Table 3). In the first step, spectral indices were derived from the SRC bands to enhance the spectral information of soil models. To test the influence of various spectral indices on the predictions, we used the standardized catalog provided by Montero et al. (2023), referencing more than 200 entries. Based on the catalog, a forward features selection (H. Meyer et al., 2019) was conducted to reduce the number of features and to identify the three most important indices for each model (Table 3). Next, band-wise spectral temporal metrics (STM) were generated by deriving the mean reflectance of the full Sentinel-2 time series without applying SRC thresholds. To reduce the number of features and avoid overfitting, only the bands with the highest correlations to SOCS (REDEGE1) and clay (SWIR2) were considered for the corresponding models (see section 2.4.2). In the last step, a 10-meter digital

elevation model (DEM) was incorporated as the only non-optical EO covariate (BKG, 2024). All model features share a common resolution of 10×10 meters (Table 3).

To assess the influence of the additional covariates and original SRC bands on model results, the feature importance was analyzed according to the permutation method described by Fisher et al. (2019). The permutation feature importance works by randomly shuffling the values of specific features while keeping the remaining features unchanged. Based on the modified datasets, predictions are carried out using a pre-trained model, and the feature importance is estimated as the difference in model performance before and after shuffling.

Table 3: Overview of the Sentinel-2 SRC bands and additional features used for the SOCS and clay models.

Name	Abb.	Equation	Model	Reference
<i>Soil Reflectance Composite Bands (SRC)</i>				
Blue (492 nm)	BLUE	$\overline{B2_{soil}}$	SOCS, Clay	-
Green (560 nm)	GREEN	$\overline{B3_{soil}}$	SOCS, Clay	-
Red (665 nm)	RED	$\overline{B4_{soil}}$	SOCS, Clay	-
Red edge (704 nm)	RE1	$\overline{B5_{soil}}$	SOCS, Clay	-
Red edge (741 nm)	RE2	$\overline{B6_{soil}}$	SOCS, Clay	-
Red edge (783 nm)	RE3	$\overline{B7_{soil}}$	SOCS, Clay	-
Broad NIR (833 nm)	BNIR	$\overline{B8_{soil}}$	SOCS, Clay	-
NIR (865 nm)	NIR	$\overline{B8a_{soil}}$	SOCS, Clay	-
SWIR1 (1614 nm)	SWIR1	$\overline{B11_{soil}}$	SOCS, Clay	-
SWIR2 (2202 nm)	SWIR2	$\overline{B12_{soil}}$	SOCS, Clay	-
<i>Soil Reflectance Composite (SRC) Indices</i>				
Normalized Difference Yellowness Index	NDYI	$\frac{\overline{B3_{soil}} - \overline{B2_{soil}}}{\overline{B3_{soil}} + \overline{B2_{soil}}}$	SOCS	Sulik & Long (2016)
Modified Bare Soil Index	MBI	$\frac{\overline{B11_{soil}} - \overline{B12_{soil}} - \overline{B8_{soil}}}{\overline{B11_{soil}} - \overline{B12_{soil}} - \overline{B8_{soil}}} + 0.5$	SOCS	Nguyen et al. (2021)
Excess Red Index	ExR	$1.3 \times \overline{B4_{soil}} - \overline{B3_{soil}}$	SOCS	G. E. Meyer et al. (1999)
Normalized Burn Ratio 2	NBR2	$\frac{\overline{B11_{soil}} - \overline{B12_{soil}}}{\overline{B11_{soil}} + \overline{B12_{soil}}}$	Clay	Van Deventer et al. (1997)
Simple Ratio (555/750 nm)	SR555	$\frac{\overline{B6_{soil}}}{\overline{B3_{soil}}}$	Clay	Gitelson & Merzlyak (1994)
Blue Normalized Difference Vegetation Index	BNDVI	$\frac{\overline{B8_{soil}} - \overline{B2_{soil}}}{\overline{B8_{soil}} + \overline{B2_{soil}}}$	Clay	Wang et al. (2007)
<i>Spectral Temporal Metrics (STM)</i>				
Vegetation red edge (704 nm)	STM_RE1	$\overline{B5_{all}}$	SOCS	-
SWIR2 (2202 nm)	STM_SWIR2	$\overline{B12_{all}}$	Clay	-
<i>Digital Elevation Model (DEM)</i>				
10 Meter Elevation Model	DEM	-	SOCS, Clay	BKG (2024)

2.6 Training Data Balancing

We developed a framework to evaluate whether data balancing affects model performance and improves the alignment between the range of predicted and observed soil properties. Like the ‘Synthetic Minority Over-sampling Technique’ (SMOTE) (Chawla et al., 2002), our proposed method balances the training data by combining minority over-sampling with majority under-sampling, following a three-step process (Fig. 3). First, the total number of training samples is extended by extracting the input features from a 3 by 3 pixel grid, instead of only using one pixel from the sample coordinates. This step is comparable to the data augmentation in SMOTE but utilizes the spectral information of the adjacent pixels instead of generating synthetic training data. Next, the balancing is conducted by assigning sampling weights to each data point based on an inverted histogram (Fig. 3) to ensure that underrepresented soil properties are more likely to be included in the training data. Nine random subsamples with different sizes between 10 and 90% of the total training samples are drawn to reflect a trade-off between strong balancing with a small sample size and weak balancing with a large sample size (Fig. 3). To identify the optimal balancing strategy for the prediction of SOCS and clay, each of the nine training sets (10-90%) was used to conduct a separate SVM (see section 2.4.2). In the final step, the results were evaluated in terms of model accuracy and prediction fit, using the original, imbalanced sampling data (Fig. 3).

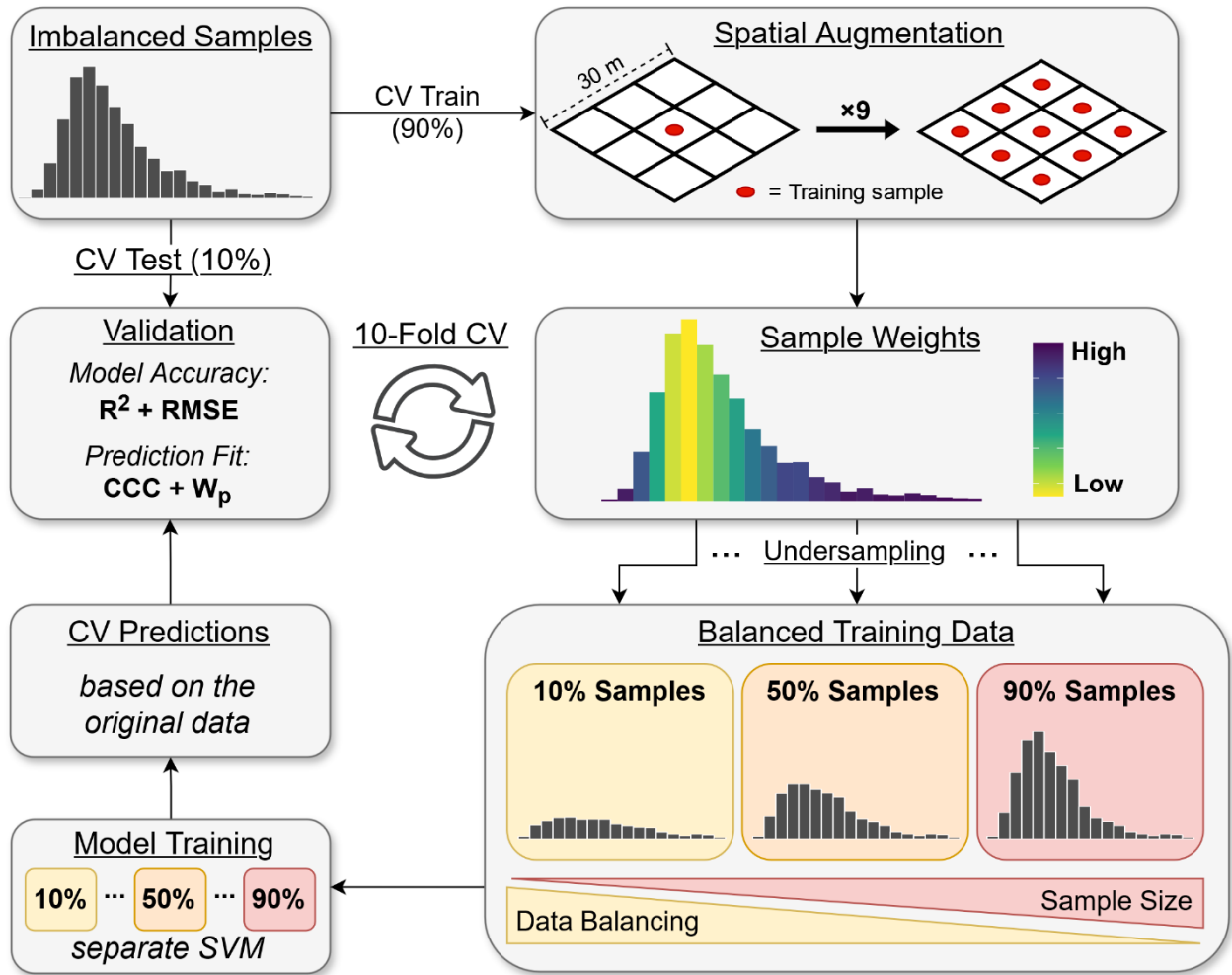


Figure 3: Flowchart of the proposed data balancing framework, tested for the prediction of SOCS and clay. The yellow and red colors reflect the trade-off between data balancing and sample size. RMSE = root mean square error; CCC = Lin's concordance correlation coefficient; W_p = Wasserstein distance.

2.7 Accuracy Assessment

The accuracy assessment for the prediction of SOCS and clay was conducted based on a 10-fold cross-validation. As shown in Fig. 3, the validation folds were always excluded from the training samples before data augmentation, ensuring that no sites were used for both training and validation. Based on the ten cross-validation folds, the linear regression (R^2) and root mean square error (RMSE) were calculated to quantify the overall accuracy of the predictions. In addition, Lin's concordance correlation coefficient (CCC) was derived to provide further details about the

agreement between the measured and predicted values (Lin, 1989). In contrast to the R^2 , the CCC also takes into account the position of the regression line, assigning higher values to predictions that are closer to the optimal 1:1 line. In the final step, the W_p was derived to quantify the distance between the distributions of measurements and predictions (see section 2.4.2). Low W_p values indicate that the model was able to accurately reproduce the distribution of the measured SOC Sand clay samples, while higher W_p values hint at the presence of over- or underrepresentations in the predictions.

2.8 Final Predictions and Uncertainty Maps

Final maps were produced for SOCS and clay content using the best-performing SRC (see section 2.4.2), the optimized data balancing (see section 2.6), and the covariates described in Table 4. For both soil properties, SVM were trained using a radial kernel and the following hyperparameters: $\epsilon = 0.1$; $\text{cost} = 1$. Spatial predictions were carried out using the R packages *mlr3* (Lang et al., 2019), *mlr3spatial* (Becker & Schratz, 2024), and *terra* (Hijmans, 2025). In addition to the final predictions, uncertainty maps were generated based on the cross-validation models. For each fold, a separate map was generated using the methods described above, and the pixel-wise uncertainty was derived using the radius of the 95 % prediction intervals (i.e., $\text{standard deviation} \times 1.96$).

3 Results

3.1 Predictive Power of the SRC

In general, strong relationships were found between all four generated SRC and the observed soil properties (Fig. 4a). For SOCS, the strongest correlations occur in the RED-NIR spectrum ($R^2 > 0.4$), while moderate relationships have been found across all bands. In contrast, the clay content shows a much more selective dependence, which is limited to the SWIR spectrum ($R^2 > 0.3$). This observed trend was consistent across all SRC, however, the magnitude of the relationships varies significantly. SRC1 and SRC2, which were both generated using low NDVI thresholds (0.25), show a noticeably lower correlation to SOCS in comparison to the other SRC (Fig. 4). Similarly, SRC1 and SRC3 were generated using low NBR2 thresholds (0.1) and showed slightly weaker correlations to clay in the SWIR2. The SRC4, based on the PV+IR2 (<0.24), consistently showed the highest correlations with SOCS across all bands, while SRC4 and SRC2 produced similar R^2 values with clay in the SWIR2 region (Fig. 4a).

This overall tendency is supported by the results of the SVM, which were trained using all SRC bands (Fig. 4a). In general, SRC4 achieved the highest model accuracy for SOCS ($CCC \approx 0.74$), followed by SRC3. In contrast, SRC1 and SRC2 show a significantly lower performance with CCC values around 0.65. For the prediction of clay, the observed patterns are slightly different. While SRC4 still produced the most accurate model ($CCC \approx 0.82$), SRC2 showed a slightly higher accuracy compared to the remaining SRC.

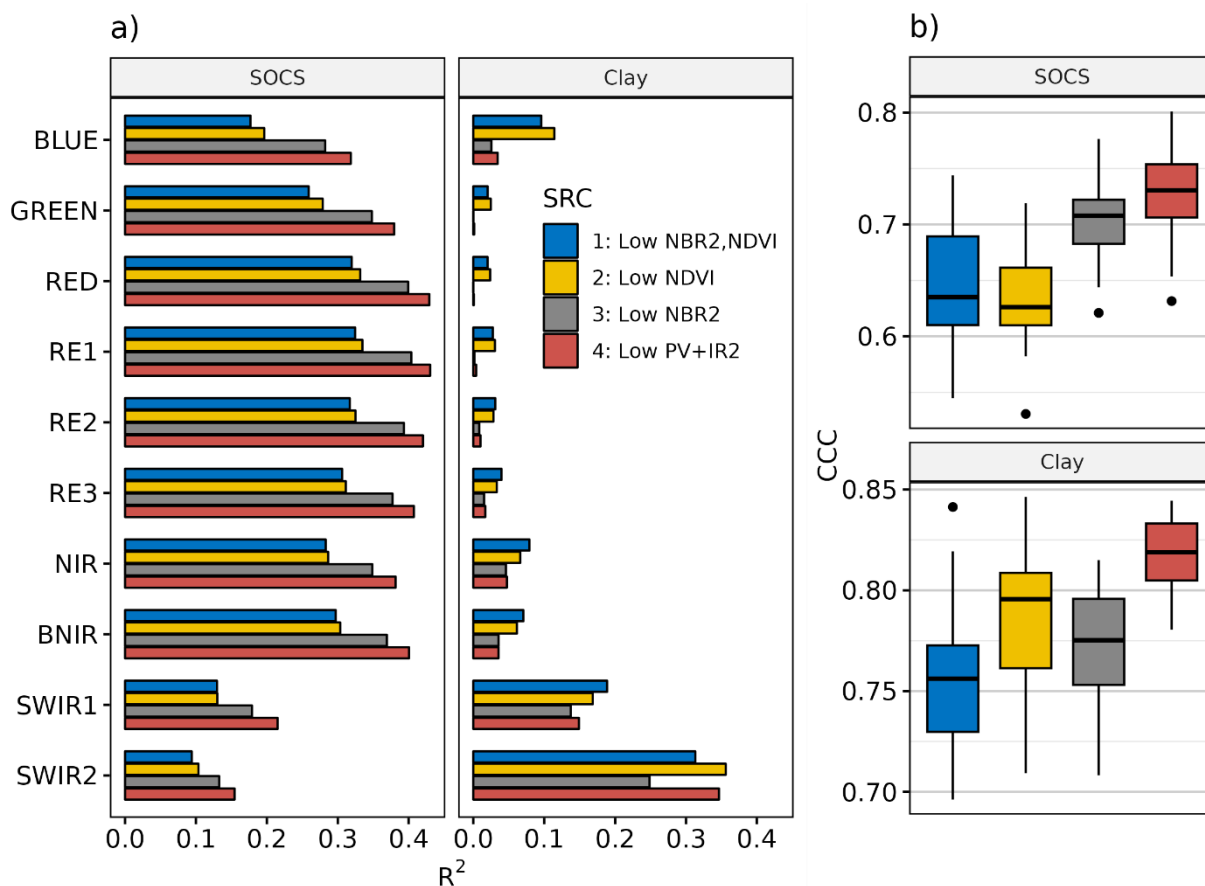


Figure 4: a) Band-wise regressions (R^2) between the four generated Sentinel-2 SRC and the corresponding SOCS and clay samples. b) Model accuracy (CCC) of each SRC for the prediction of SOCS and clay, based on the ten Sentinel-2 bands.

3.2 Dependencies between Soil Properties and Bare Soil Indices

Across the generated SRC, strong positive correlations were observed between NBR2 and clay content (Fig. 5a). The highest relations were found for SRC4 ($R^2 = 0.54$) and SRC2 ($R^2 = 0.47$) which both utilize high NBR2 thresholds (0.16), as illustrated by the dashed lines in Fig. 5a. In

contrast, the low NBR2 thresholds (<0.1) used for the generation of SRC1 and SRC3 significantly reduced the range of NBR2 values, strongly decreasing the observed correlations ($R^2 = 0.44$ and 0.41 respectively). A similar, but slightly weaker relationship was found between NDVI and SOCS (Fig. 5d). In this case, the strongest correlation was observed for SRC4 ($R^2 = 0.29$), followed by SRC3 ($R^2 = 0.23$). Again, the SRC utilizing low NDVI thresholds (SRC1 and SRC2) generally showed a restricted range and a lower correlation of around 0.14 . In addition to these strong correlations, a local dependency was found between NDVI and clay contents below 20%, which is most pronounced in SRC3 and SRC4 (Fig. 5c). Weak relationships ($R^2 < 0.14$) were found between clay and PV+IR2, but are limited to SRC2 and SRC4 (Fig. 5e). Across all four observed SRC, no significant correlations were observed between NBR2, PV+IR2, and SOCS (Fig. 5b+f)

To identify potential spatial dependencies and patterns in the results, the three observed bare soil indices were calculated for the whole research area using the results from SRC4 (Fig. 5). For the NDVI, a strong spatial clustering is visible, with the highest values being present in Northwest Germany. The NBR2 shows a clear gradient across the research areas, with low values in the north that are increasing towards the south. In comparison, the PV+IR2 generally shows a much more homogeneous distribution across the research area, although slight spatial variability is visible, especially in floodplains with elevated soil moisture levels.

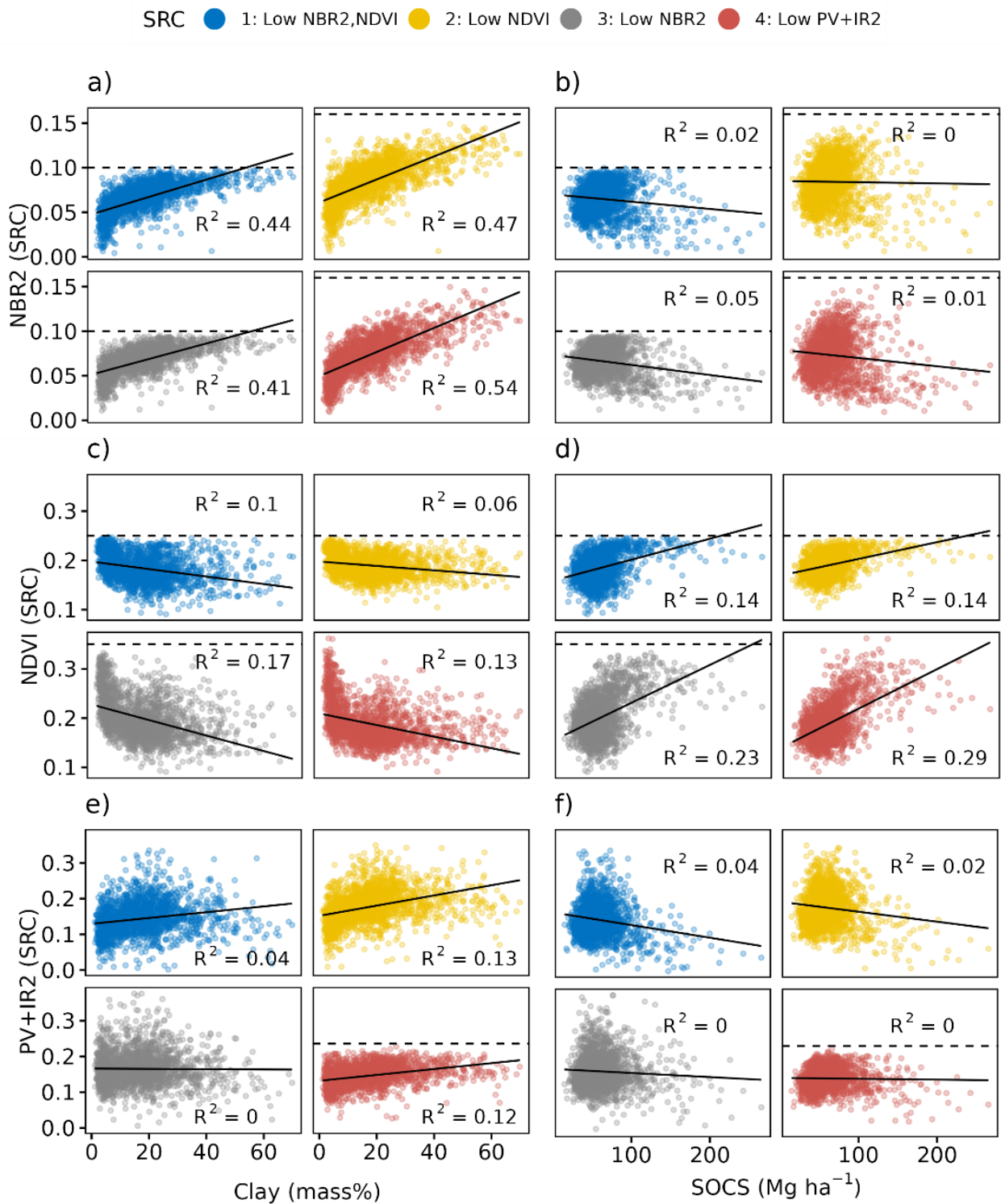


Figure 5: Regressions (R^2) between the bare soil indices (NBR2, NDVI, and PV+IR2) derived from the SRC bands, and the observed soil properties (Clay and SOCS). Black lines = linear regressions; Dashed lines indicate SRC thresholds.

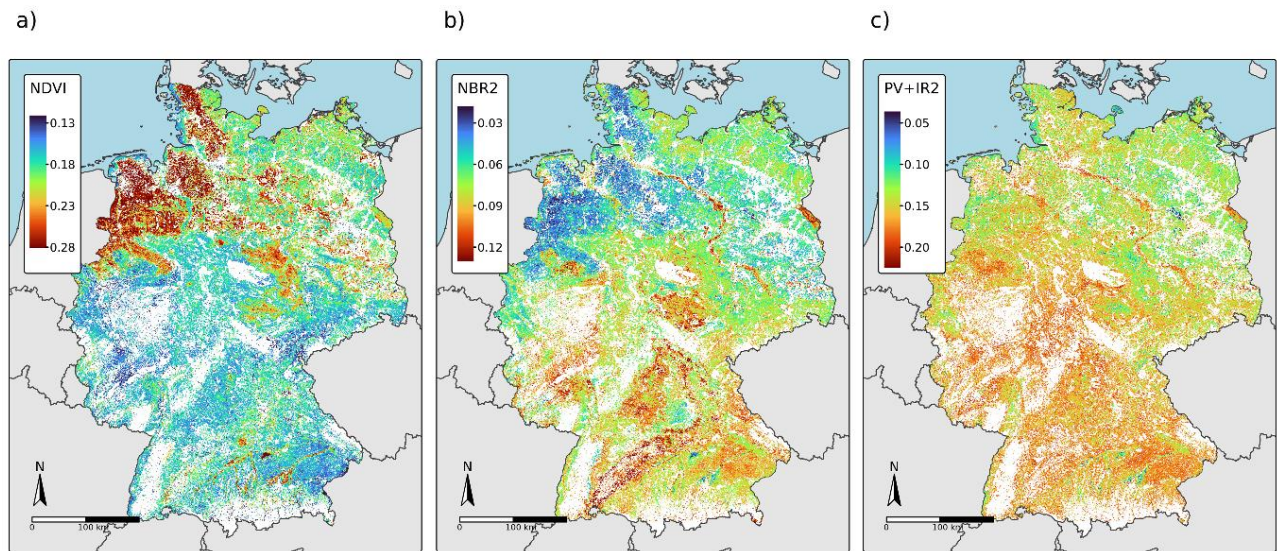


Figure 6: Maps of the bare soil NDVI (a), NBR2 (b), and PV+IR2 (c) in Germany, based on the results from SRC4.

3.3 Comparison of Included and Excluded Samples

In addition to quantifying the predictive power of each SRC, we evaluated the distributions of the included and excluded samples to identify potential bias (Fig. 7). For SOCS, the highest agreements between the values above and below the SRC thresholds were found in SRC4 ($W_p = 0.3$) and SRC3 ($W_p = 0.44$). In contrast, the SRC1 and 2 showed much lower agreements, with W_p values above 0.8. In these cases, high SOCS values were excluded more frequently, altering the distributions when compared to the soil samples.

Significant differences were also observed in the distributions of the clay content (Fig. 7). Again, the highest agreement between included and excluded samples was found for SRC4 ($W_p = 0.17$), suggesting the lowest bias in the representation of the clay content. In contrast, the distributions show that SRC3 disproportionately excluded samples with high clay values, which significantly increased the W_p to 0.9. Similarly, SRC2 led to the exclusion of samples with low clay values ($W_p = 0.45$), while SRC1 showed a combination of both exclusion patterns ($W_p = 0.52$).

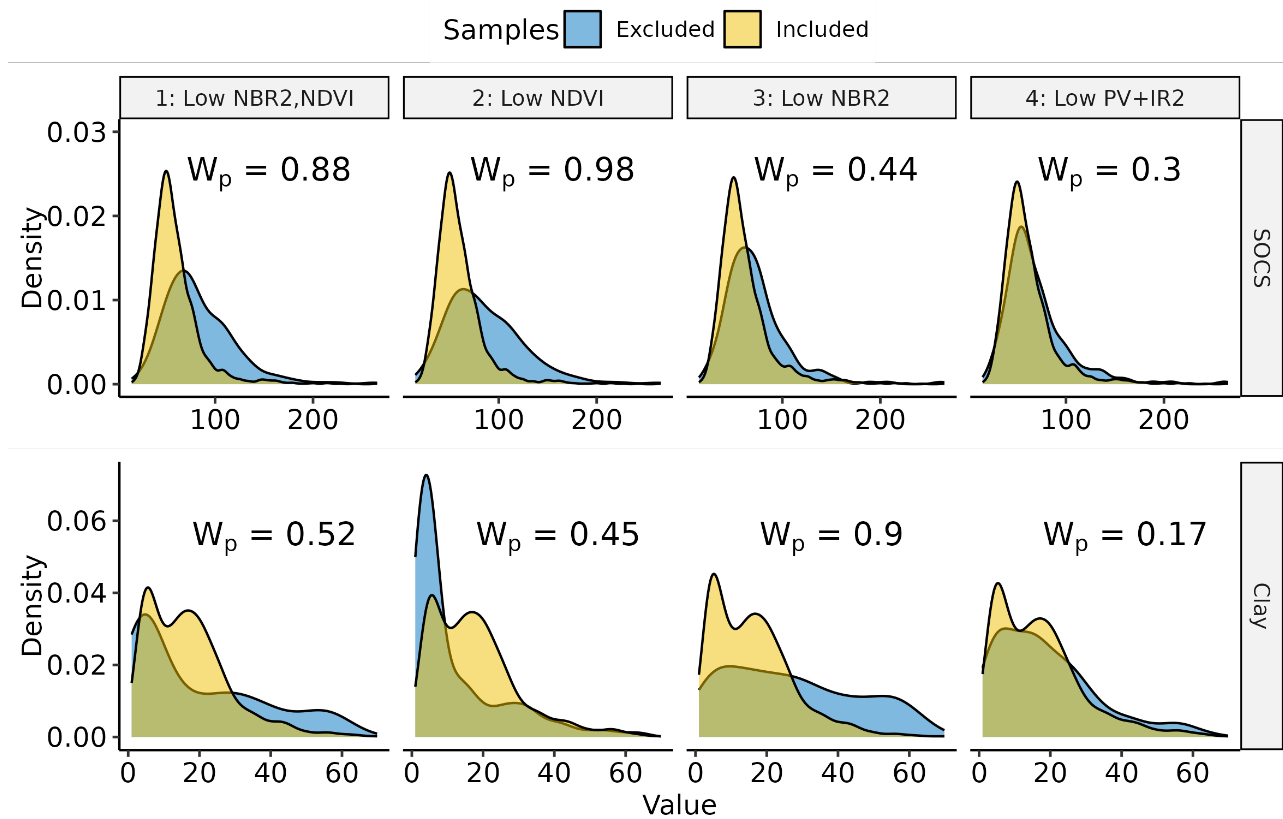


Figure 7: Density plots of the SOCS/clay samples that were included (yellow) and excluded (blue) by the corresponding SRC. For each SRC, the proportion of soil samples below the thresholds is around 90% (see Table 3)

3.4 Model Performance and Influence of Additional Features

Based on the fact that SRC4 (PV+IR2 < 0.24 & NBR2 < 0.16) showed the highest predictive power (Fig. 4b) and lowest W_p values/bias (Fig. 7), it was used for further analyses of the model performance. Comparing the results of the baseline models, trained on the SRC bands only, the prediction of clay (Fig. 8a) achieved slightly higher accuracy than SOCS (Fig. 9a) ($R^2 = 0.72$ and 0.61, respectively). As illustrated by the regression lines, the SOCS model showed a slightly stronger tendency to underpredict high values, which is reflected by the CCC values (SOCS = 0.74; clay = 0.82). In general, the observed SOCS distribution of the baseline model was significantly narrower compared to the measurements, resulting in a relatively high W_p of 0.19 (Fig. 8a). Similarly, extreme values were underrepresented in predictions of the clay model, shifting the distribution toward the mean and increasing the W_p (0.15) (Fig. 9a).

Including additional EO-based features significantly increased the prediction accuracy for both SOCS (CCC = 0.78) and clay (CCC = 0.88) (Fig. 8b & Fig. 9b). In both cases, these enhancements were also visible in the distributions of predicted values. In the clay model, the W_p strongly improved from 0.15 to 0.09, aligning the predictions more closely with the measured value range. While the addition of covariates also slightly reduced the W_p of the SOCS predictions (0.19 to 0.16), the models' limitation to reproduce the full range distribution of the measurements remained.

The analysis of the permutation feature importance revealed that the SRC bands and indices were by far the most influential covariates for the prediction of clay, with a relative RMSE loss of around 150% (Fig. 10). While the SRC features (bands + indices) were also the most influential covariates in the SOCS model, the observed magnitude of the permutation performance was much smaller, with values below 50%. Unlike the SRC, the inclusion of STM showed moderate importance for the prediction of SOCS, while it had no impact on the clay model. In both cases, a similar level of importance was assigned to the DEM, though its influence was significantly weaker compared to features based on the SRC.

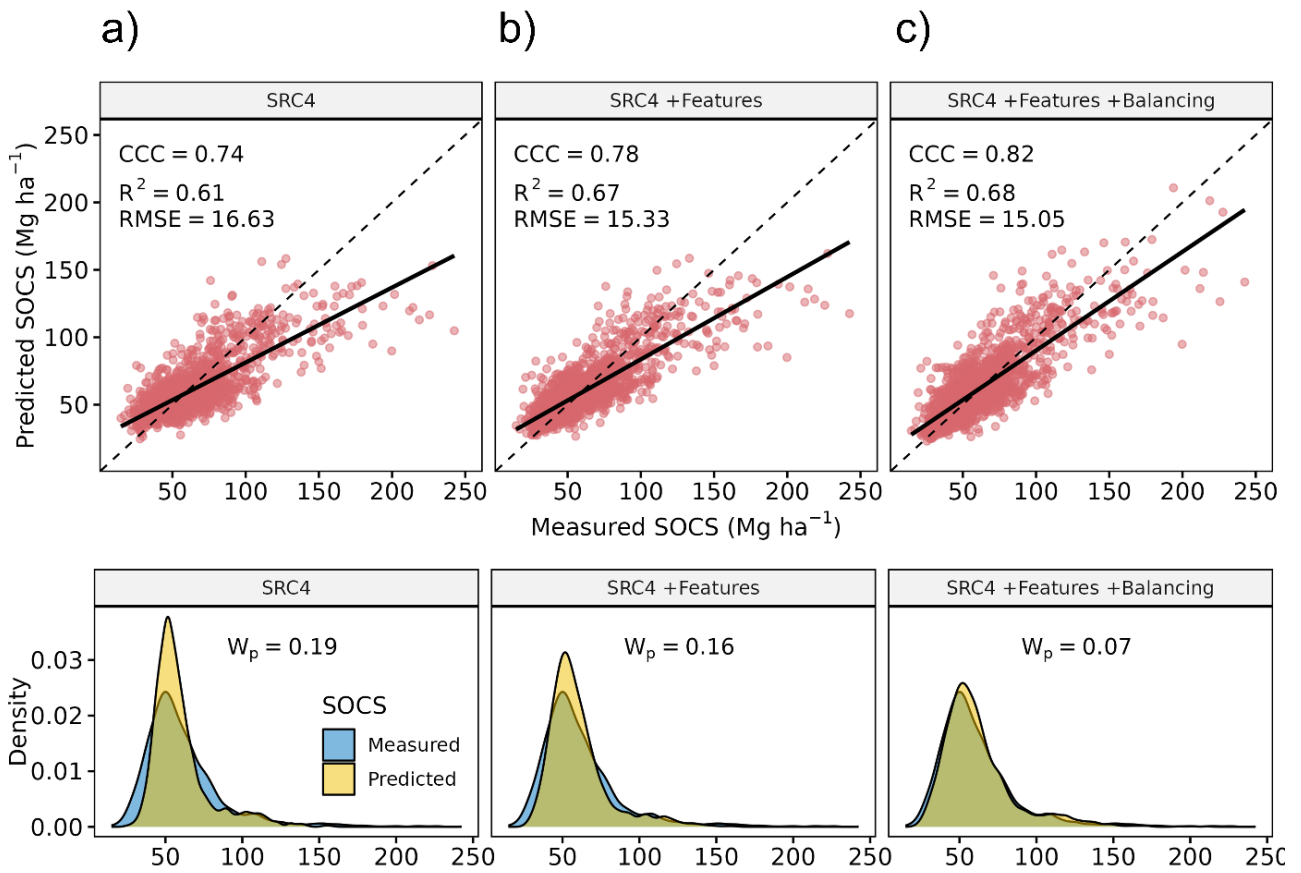


Figure 8: (Top) Comparison of the SOCS model performance using the SRC bands only (a), the SRC bands in combination with additional features (b), and the SRC bands with features and optimal data balancing (c). Black lines = linear regressions; dashed lines = 1:1 line. (Bottom) Corresponding density plots and W_p values of the measured (blue) and predicted (yellow) SOCS values.

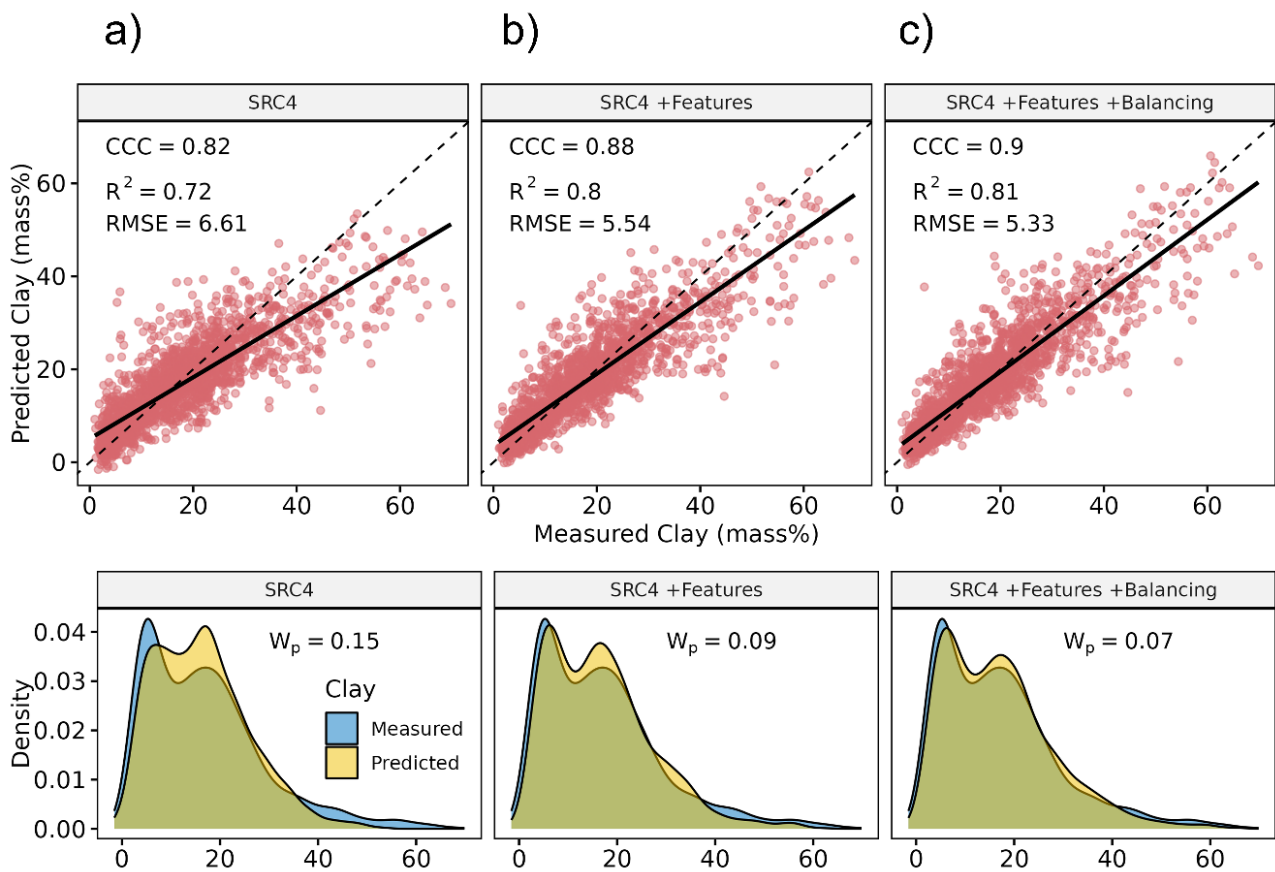


Figure 9: (Top) Comparison of the clay model performance using the SRC bands only (a), the SRC bands in combination with additional features (b), and the SRC bands with features and optimal data balancing (c). Black lines = linear regressions; dashed lines = 1:1 line. (Bottom) Corresponding density plots and W_p values of the measured (blue) and predicted (yellow) clay values.

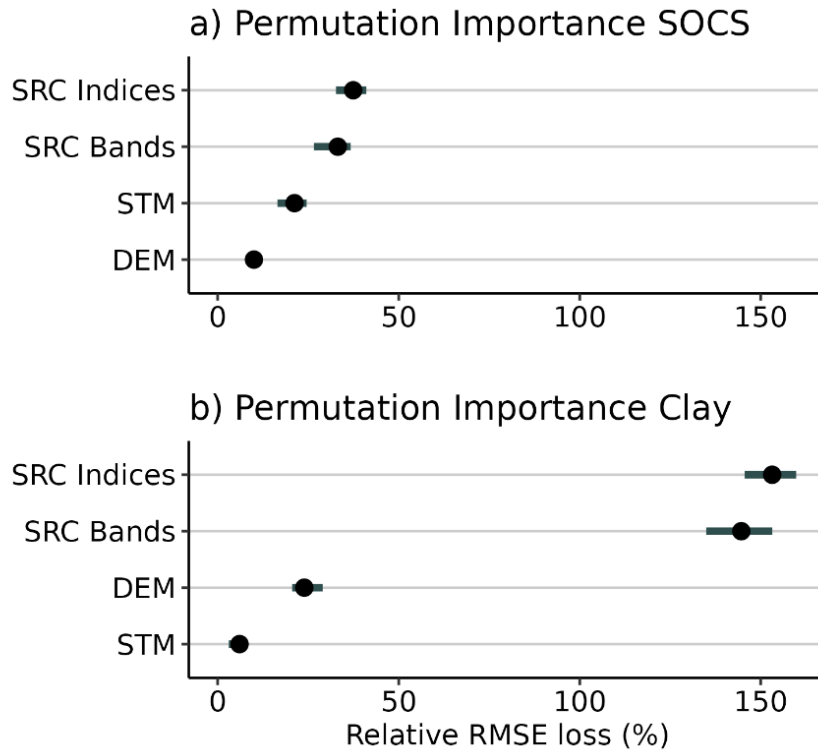


Figure 10: Relative feature importance (permutation loss) of the covariate groups (Table 4) for the prediction of SOCS (a) and clay (b). STM = Spectral temporal metrics; DEM = Digital elevation model.

3.5 Effects of the Data Balancing on the Model Performance

We expanded the training dataset using a spatial augmentation approach (Fig. 3) to evaluate the influence of data balancing on the model performance. For the prediction of SOCS, a clear trade-off emerged between training data size and balancing (Fig. 11a). Models based on strong balancing (i.e., using only 10% of the samples) showed significantly higher RMSE values, indicating a tendency to overpredict SOCS. With increasing sample size, the overall accuracy improved, reaching an optimum when using intermediate balancing and around 30% of the training samples. While the models based on the weak balancing (i.e., 90 %) produced similar R^2 and RMSE values, the performance of the CCC and W_p was significantly lower. A similar trend was observed for the clay model, though the optimal trade-off between data size and balancing was higher at around 60% (Fig. 11b).

The final predictions based on the optimal data balancing for SOCS (30 %) and clay (60 %) are shown in Fig. 8c & Fig. 9b. In both models, the data augmentation and balancing increased the CCC from 0.78 to 0.82 (SOCS) and 0.88 to 0.9 (clay), shifting the regressions closer to the optimal 1:1 line. In addition to the CCC, minor improvements were also observed in the RMSE and R^2 values. While the data balancing also improved the distributions of the predictions in both cases, the reduction of the W_p was more significant for the SOCS ($W_p = 0.16$ to 0.07) than for clay ($W_p = 0.09$ to 0.07).

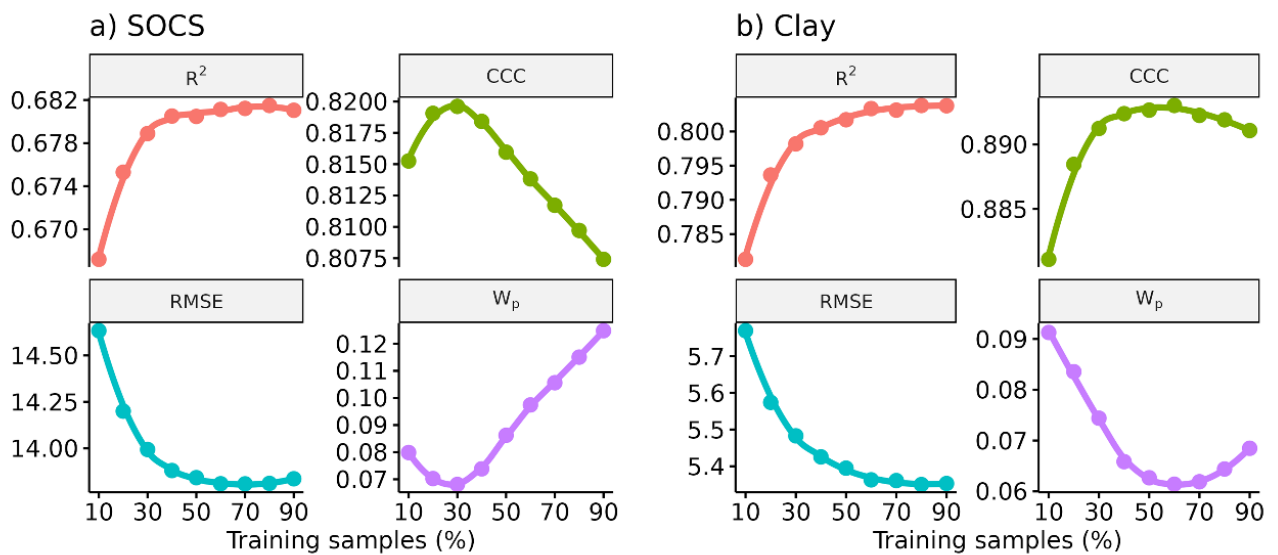


Figure 11: Influence of data balancing (i.e., percent of training samples included) on the model accuracies (R^2 , RMSE, CCC, W_p) for the prediction of SOCS (a) and clay (b). Small sample size = strong balancing; Large sample size = weak balancing (see Figure 3).

3.6 Final Predictions and Uncertainty Maps

Based on the final models, predictions were carried out to map cropland SOCS (Fig. 12) and clay (Fig. 13) in Germany. The Northern Plain can be divided into two regions, exhibiting soils with low SOCS and clay in the east, while the western parts predominantly show soils with high SOCS and low clay. Regions with high SOCS and clay are mostly found in the Loess Hills and the Southern Scarplands. The Western Highlands are characterized by soils with low SOCS and medium to high

clay, while regions with medium and high SOCS and clay are mostly present in the Eastern Highlands and Alpine Foreland.

To provide further information on the predictions of SOCS and clay, uncertainty maps were generated based on cross-validation models (Fig. 14). For the former, the highest uncertainties were present in Northwest and South Germany, corresponding to the regions with the highest SOCS predictions (Fig. 14a). In addition, increased uncertainties were also found in parts of Central and Southern Germany, which are characterized by high clay contents (Fig. 13). In contrast, the uncertainty map for clay (Fig. 14b) is similar to the overall prediction map and is not influenced by the presence of SOCS. In this case, increased uncertainties are connected to floodplains and similar regions with elevated levels of soil moisture.

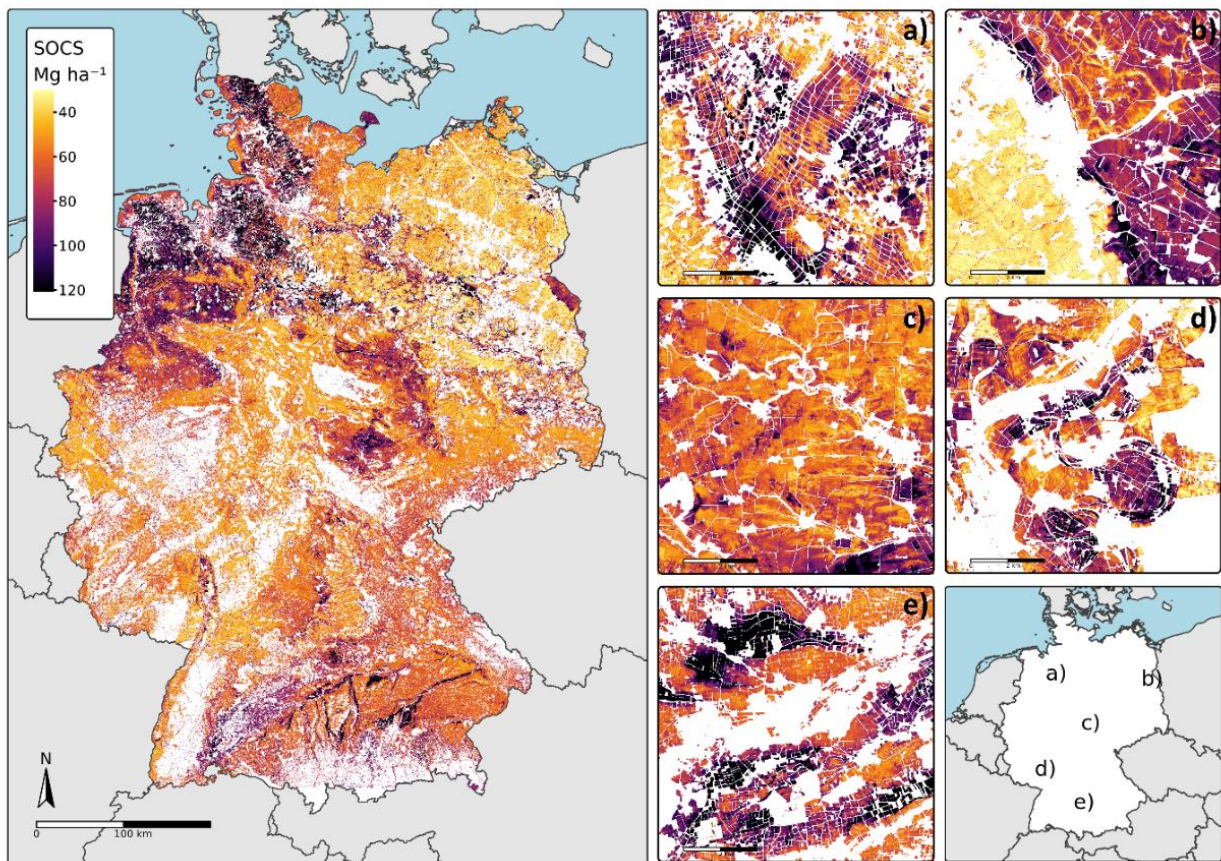


Figure 12: Final prediction map of the cropland SOCS (0 – 30 cm) in Germany.

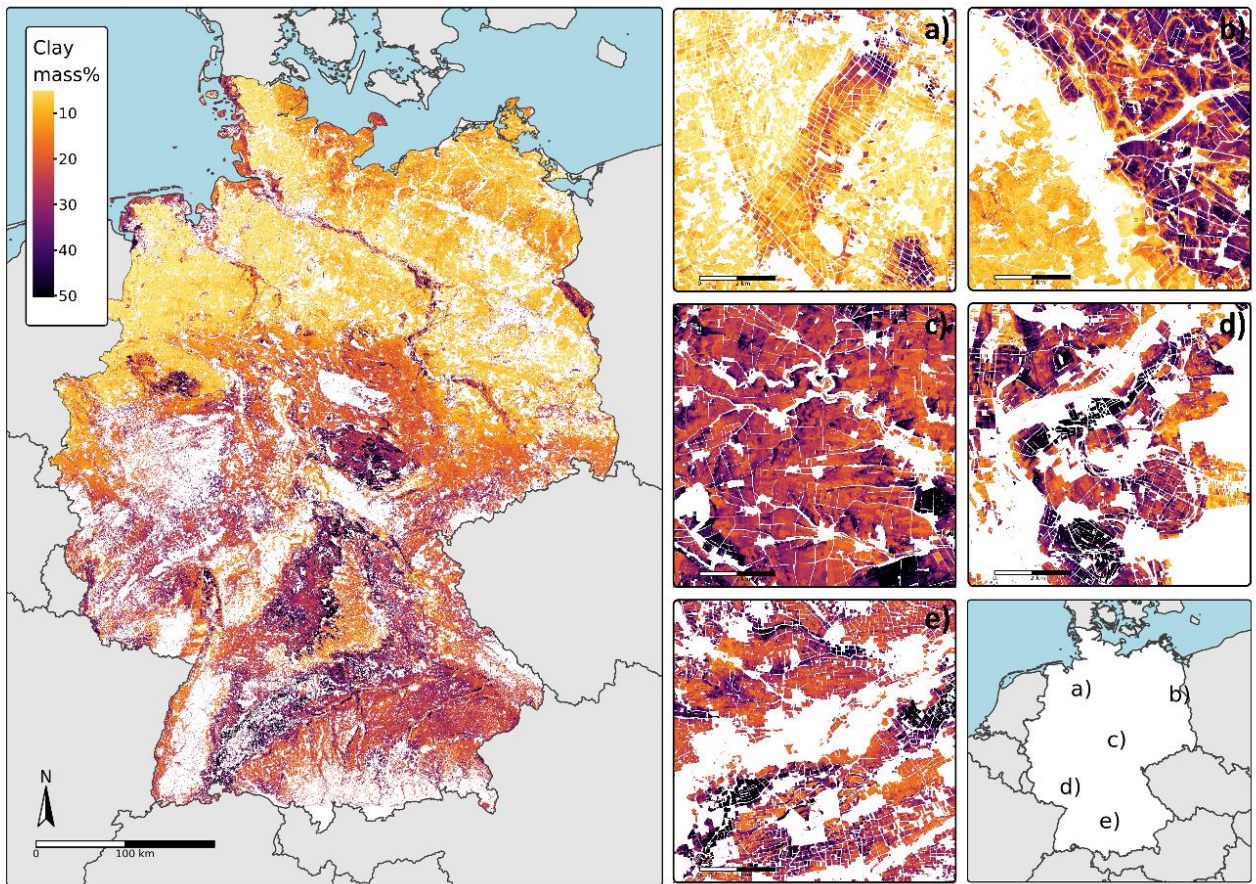
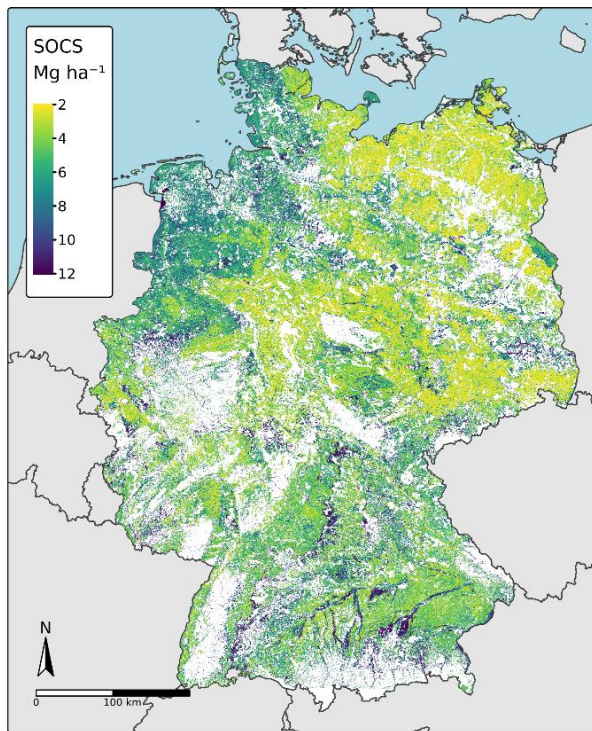


Figure 13: Final prediction map of the cropland clay content (0–30 cm) in Germany.

a) Prediction Uncertainty SOCS



b) Prediction Uncertainty Clay

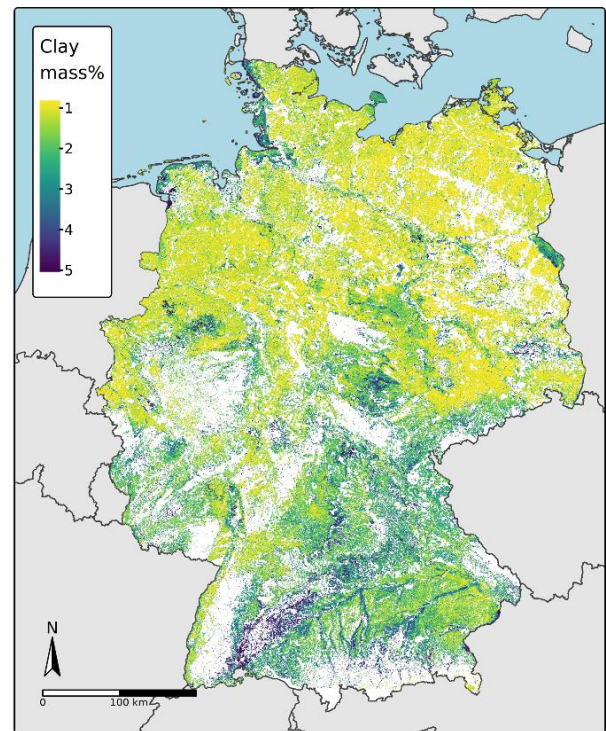


Figure 14: Prediction uncertainty for SOCS (a) and clay (b), based on the cross-validation models.

4 Discussion

4.1 Influence of Bare Soil Indices on the SRC

Our results indicate that the NDVI and NBR2, which are often used to generate SRC (Delaney et al., 2025), are strongly related to the bare soil reflectance and the presence of SOCS and clay. The relationship between NBR2 and clay content is significantly more pronounced ($R^2 = 0.54$) compared to the underlying SRC Bands (Fig. 4 & Fig. 5). These findings align with previous EO-based studies and soil spectroscopy, showing that SWIR bands are particularly sensitive to the presence of clay minerals (Chabrillat et al., 2019; Shabou et al., 2015; Wetterlind et al., 2025). Similarly, the observed correlation between NDVI and SOC ($R^2 = 0.29$) can be explained by studies showing that “dark” (i.e., carbon-rich) soil substrates produce higher NDVI values than “bright” soils, given the same presence of vegetation (Huete, 1988).

Directly comparing different parameter combinations, we were able to demonstrate that low NBR2 (0.1) and NDVI (0.25) thresholds significantly affect the distributions of the soil samples that are included and excluded by the SRC. As illustrated in Fig. 7, low NBR2 thresholds strongly favor the selection of samples with lower clay content (SRC1, SRC3), while a similar effect was observed for low NDVI thresholds and high SOCS values (SRC1, SRC2). The corresponding W_p values underline that the implementation of such thresholds to generate SRC introduces systematic bias by excluding certain soil parameters from the resulting maps (Fig. 7). These dependencies are also reflected in the spatial distribution of NDVI and NBR2 (Fig. 6) showing that both indices are clustered in soil regions with high SOCS or clay values.

Given these clear dependencies, it is surprising that many studies still rely on low NDVI or NBR2 thresholds when generating SRC for soil mapping applications (Castaldi et al., 2019; Demattê et al., 2025; Silvero et al., 2021). One reason is that these dependencies are overlooked when focusing on individual soil properties to optimize the SRC and resulting maps. No direct correlation was found between NBR2 and SOCS (Fig. 5) and it would be much more difficult to detect the underlying bias when only comparing SOCS distributions of the included and excluded samples (e.g. in SRC3 in Fig. 7). In addition, a biased selection of soil samples for training can also enhance the apparent model performance in some cases, making it less obvious and harder to detect. This is supported by several studies, reporting that the SOC prediction accuracy increased when using very low NBR2 thresholds to generate SRC, while also significantly reducing the number of training samples (Castaldi et al., 2019; Dvorakova et al., 2022; Vaudour et al., 2021). Our findings suggest, however, that this effect is strongly influenced by the systematic exclusion of soil samples with high clay contents, which are known to interfere with the prediction of SOC (Stenberg, 2010). This effect is supported by Fig. 14a, highlighting that the highest prediction uncertainties for SOCS are located in regions with clayey soils.

To minimize the bias in the final soil maps, it is recommended to compare the distributions of multiple soil properties, even the ones that are not included in the models (Fig. 7). In general, the scatter plots in Fig. 5 show the high NDVI or NBR2 thresholds exclude fewer samples and are less likely to introduce bias for soil modeling. If applying low thresholds to reduce the influence of vegetation cover instead, it is strongly suggested to rely on bare soil indices that are not affected by the soil reflectance itself. Heiden et al. (2022) found that while the NBR2 provided the highest SRC quality, the PV+IR2 was better suited to differentiate bare soil from vegetated soil and provided the

best SRC masking. This is supported by our findings, showing that the PV+IR2 is affected less by the observed soil properties, preserving the original distributions of the SOCS and clay samples to a high degree (Fig. 7).

4.2 Influence of the SRC on the Prediction of SOCS and Clay

Despite being recommended in the literature (Demattê et al., 2020), our findings show that SRC1 based on low NDVI (<0.25) and NBR2 (<0.1) thresholds yielded the lowest overall model performance to predict SOCS and clay (Fig. 4). Instead, significantly higher accuracies were achieved using SRC4 (PV+IR2 < 0.24 & NBR2 < 0.16), highlighting the importance of the SRC settings on the model results. Analyzing the dependencies between the SRC bands and soil properties, we were able to attribute these findings to two key factors. As noted by several studies, the NDVI lacks sufficient spectral information to effectively differentiate bare soil from vegetation cover, especially in the presence of crop residues (Castaldi et al., 2023; Demattê et al., 2018). It has been shown that in spectrally mixed regions (bare soil, vegetation, residues), the NDVI produced the lowest performance out of the observed bare soil indices and should, therefore, not be used to generate SRC for soil mapping (Heiden et al. 2022). Consequently, our findings underline that the SRC based on low NDVI thresholds (SRC1 and SRC2) exhibited significantly weaker correlations with SOC across all bands, suggesting a lower spectral quality.

In contrast, it has been suggested that NBR2 is highly sensitive toward the presence of non-photosynthetic vegetation and effective in detecting optimal bare soil observations (Dvorakova et al., 2022). Our results indicate, however, that the positive influence of low NBR2 thresholds on the prediction of SOC does not apply under all circumstances. When using the same NBR2 threshold (0.1) across different SRC, we found that increasing the NDVI threshold from 0.25 (SRC1) to 0.35 (SRC3) significantly improved the accuracy of the SOCS model (Fig. 4). This improvement can be explained by the systematic exclusion of high-SOCS samples in SRC1 ($>80 \text{ Mg h}^{-1}$), restricting the range of SOCS values and weakening the overall model regression (Fig. 5 & Fig. 7). As noted in the previous section, it is questionable if the positive influence of low NBR2 thresholds on SOCS prediction truly results from an improved selection of bare soil observations or is caused by the systematic exclusion of clayey soils. This is supported by the fact that the improved performance of SRC3 (NBR2 <0.1 & NDVI <0.35) did not extend to the clay model and is strongly influenced by

the removal of high-clay samples above 30 mass% (Fig. 4 & Fig. 7). In general, our findings show that SRC4 yielded the highest accuracy for both models, which is supported by the results of Heiden et al. (2022) (Fig. 4). Considering the high dependence between the bare soil indices and soil properties (Fig. 7), however, we were able to demonstrate that a direct comparison of different SRC is only valid when also taking into account the samples that have been excluded by the thresholds.

4.3 Model Performance and Feature Importance

The baseline models, trained using the ten SRC bands only, produced good accuracies for the prediction of SOCS and clay, which are comparable to other large-scale soil property maps (Chen et al., 2022). Similar to other studies based on SRC (Silvero et al., 2021; Stumpf et al., 2024; Žižala et al., 2022), the model performance was slightly better for clay than for SOCS, which can be explained by several factors. First, it is well-documented that clay minerals influence the reflectance in the SWIR region (Chabrillat et al., 2019; Wetterlind et al., 2025), which is supported by the strong correlation between NBR2 (i.e, the normalized SWIR-ratio) and clay (Fig. 5). Even though SOC affects a much broader spectrum (Fig. 4), the correlation is slightly lower, reducing the predictive power of the SRC compared to clay. A simple explanation for this tendency is the fact that clay usually makes up a much larger portion of the total soil mass, increasing its influence on soil reflectance as compared to SOC.

The inclusion of further EO-based covariates significantly improved the performance of both models, however, for different reasons (Fig. 8 & Fig. 9). While both models profited from additional indices based on SRC, the improvement was much more distinct for the prediction of clay (Fig. 9). This is in line with the strong influence of clay on the soil reflectance and is supported by the high magnitude of the SRC bands and indices in the permutation feature importance (Fig. 10). In contrast, our findings show that the inclusion of STM only improved the SOCS model but did not affect the prediction of clay (Fig. 10). As illustrated in Fig. 5, the “darkness” of the soil can influence vegetation indices, allowing the SOCS signal to persist in STM to some degree even when derived from the complete Sentinel-2 time series (Huete, 1988). The same does not apply to the spectral signal of clay in the SWIR range, which is strongly affected by vegetation cover and lost when deriving STM. Additional research is necessary to uncover what kind of additional information is provided by the STM to improve the SOCS prediction.

The addition of a 10-meter DEM improved both models to a similar degree, which is supported by the results of other studies (Stumpf et al., 2024; Urbina-Salazar et al., 2023; Žižala et al., 2022). It has been shown that soil properties like SOC and clay are influenced by geomorphology and that landscape features such as elevation can play in key role in DSM (Behrens et al., 2018). Given the strong north-south gradient in elevation and spatial clustering of soils in the research area (Fig. 1), it is possible that the DEM also serves as a more general spatial proxy describing the positions of the sampling locations within the research area (Hengl et al., 2018; Møller et al., 2020).

4.4 Influence of Sample Balancing and Additional Covariates

Despite achieving good results, both baseline models showed tendencies to underpredict high SOCS and high clay values (Fig. 8 & Fig. 9). Similar findings have been reported for the prediction of SOC based on SRC (Zepp et al., 2021) and are often attributed to imbalanced training data and the underrepresentation of soil samples with extreme values (Feeney et al., 2022). Comparing the measured and predicted SOCS and clay in Fig. 8 & Fig. 9, it is visible that the baseline models often predicted values close to the mean and were unable to reproduce the full range of the input data. As highlighted by Feeney et al. (2022), this tendency can be attributed to two main factors: (1) the ability of the spatial covariates to capture the full range of soil parameters, and (2) the distribution and representation of the training samples.

Our results demonstrate that both of these factors can be improved by providing further EO-based input features (Table 3) and implementing data balancing frameworks (Fig. 3), but depend on the corresponding soil parameters. While the addition of STM, DEM, and spectral indices significantly increased the overall prediction accuracy in both cases, the improvement of the W_p was more significant for clay (Fig. 8 & Fig. 9). As shown in Fig. 2, the measured SOCS is highly imbalanced with values that are concentrated around $50 \pm 20 \text{ Mg ha}^{-1}$ and few outliers above 100 Mg ha^{-1} . Our findings demonstrate that in this case, data balancing can be used to further improve the prediction fit (i.e., CCC) and the model's ability to reproduce the range and distribution of the soil samples (i.e., W_p). As highlighted in Fig. 11, however, the positive influence of our proposed method (Fig. 3) strongly depends on identifying the optimal trade-off between sample size and data balancing. In general, it can be concluded that soil properties with outliers and highly skewed distributions also require a stronger balancing (SOCS $\approx 30\%$) compared to properties with more even distributions

(clay \approx 60%) (Fig. 11). In both cases, the model improvements are most significant in the W_p and CCC, increasing the range and representation of the soil samples in the final prediction maps.

5 Conclusion

In this study, we used Sentinel-2 bare soil maps and soil monitoring data to generate national maps of cropland SOCS and clay with very high accuracy (CCC = 0.82 and 0.90, respectively). The analysis aimed to understand the impact of different bare soil indices and threshold values on the resulting SRC and soil models. Additionally, we explored whether data balancing and incorporating additional EO-based features could further improve prediction accuracy, especially when using imbalanced data sets. Our main findings demonstrate that:

- While varying SRC parameters can lead to similar model outcomes, interactions between the bare soil indices and soil parameters can significantly affect the prediction accuracy and bias of the final maps.
- Strong correlations were found between the NBR2 and clay ($R^2 = 0.54$) and NDVI and SOCS ($R^2 = 0.29$), resulting in the systematic exclusion of specific soil values when applying low thresholds to generate SRC.
- Instead of relying on NBR2 or NDVI, prioritizing bare indices that are less correlated with soil properties (e.g., PV+IR2) improves model accuracy while maintaining the distributions of the soil samples.
- While the baseline models tended to underpredict high values and failed to capture the full range of the soil samples, the addition of further EO-based features (i.e., spectral indices, STM, DEM) significantly improved prediction accuracy (R^2 , RMSE) and the alignment between the measurements and predictions (CCC, W_p).
- Data augmentation and balancing were successfully used to further improve the CCC and W_p and increase the range of the predictions, but require identifying the optimal trade-off between the size and balance of the training data.
- Based on our findings, we recommend extending the accuracy assessment of SRC-based soil property maps by (1) taking into account the excluded samples to identify potential model bias, and (2) comparing the range and distribution of the predictions and soil samples to increase the applicability and reliability of the final soil maps.

Declaration of Competing Interest

The authors declare that they have no known competing financial interests or personal relationships that could have appeared to influence the work reported in this paper.

Acknowledgements

The project “KlimaFern” is funded by the Federal Ministry of Food and Agriculture as part of the German Climate Protection Programme 2022.

Data Availability

The Sentinel-2 soil reflectance composite and predicted soil maps are available in Zenodo at <https://doi.org/10.5281/zenodo.15402687> and <https://doi.org/10.5281/zenodo.15403341>. The soil data from the German Agricultural Soil Inventory (BZE-LW) are available from OpenAgrar at <https://doi.org/10.3220/DATA20200203151139>.

Declaration of generative AI and AI-assisted technologies in the writing process

During the preparation of this work the authors used ChatGPT in order to improve the language of the manuscript. After using this tool, the authors reviewed and edited the content as needed and take full responsibility for the content of the published article.

References

- Becker, M., & Schratz, P. (2024). *mlr3spatial: Support for Spatial Objects Within the “mlr3” Ecosystem*. <https://mlr3spatial.mlr-org.com>
- Behrens, T., Schmidt, K., MacMillan, R. A., & Viscarra Rossel, R. A. (2018). Multi-scale digital soil mapping with deep learning. *Scientific Reports*, 8(1), 15244. <https://doi.org/10.1038/s41598-018-33516-6>
- BGR. (2007). *Bodenarten der Böden Deutschlands*. https://www.bgr.bund.de/DE/Themen/Boden/Informationsgrundlagen/Bodenkundliche_Karten_Datenbanken/Themenkarten/BOART1000OB/boart1000ob_node.html
- BKG. (2024). *Digitales Geländemodell Gitterweite 10 m (DGM10)*. <https://gdz.bkg.bund.de/index.php/default/digitales-gelandemodell-gitterweite-10-m-dgm10.html>
- Broeg, T., Blaschek, M., Seitz, S., Taghizadeh-Mehrjardi, R., Zepp, S., & Scholten, T. (2023). Transferability of Covariates to Predict Soil Organic Carbon in Cropland Soils. *Remote Sensing*, 15(4), Article 4. <https://doi.org/10.3390/rs15040876>
- Broeg, T., Don, A., Gocht, A., Scholten, T., Taghizadeh-Mehrjardi, R., & Erasmi, S. (2024). Using local ensemble models and Landsat bare soil composites for large-scale soil organic carbon maps in cropland. *Geoderma*, 444, 116850. <https://doi.org/10.1016/j.geoderma.2024.116850>
- Buchner, J., Yin, H., Frantz, D., Kuemmerle, T., Askerov, E., Bakuradze, T., Bleyhl, B., Elizbarashvili, N., Komarova, A., Lewińska, K. E., Rizayeva, A., Sayadyan, H., Tan, B., Tepanosyan, G., Zazanashvili, N., & Radeloff, V. C. (2020). Land-cover change in the Caucasus Mountains since 1987 based on the topographic correction of multi-temporal Landsat composites. *Remote Sensing of Environment*, 248, 111967. <https://doi.org/10.1016/j.rse.2020.111967>
- Castaldi, F., Chabrillat, S., Don, A., & van Wesemael, B. (2019). Soil Organic Carbon Mapping Using LUCAS Topsoil Database and Sentinel-2 Data: An Approach to Reduce Soil Moisture and Crop Residue Effects. *Remote Sensing*, 11(18), 2121. <https://doi.org/10.3390/rs11182121>
- Castaldi, F., Halil Koparan, M., Wetterlind, J., Žydelis, R., Vinci, I., Özge Savaş, A., Kıvrak, C., Tunçay, T., Volungevičius, J., Obber, S., Ragazzi, F., Malo, D., & Vaudour, E. (2023). Assessing the capability of Sentinel-2 time-series to estimate soil organic carbon and clay content at local scale in croplands. *ISPRS Journal of Photogrammetry and Remote Sensing*, 199, 40–60. <https://doi.org/10.1016/j.isprsjprs.2023.03.016>
- Chabrillat, S., Ben-Dor, E., Cierniewski, J., Gomez, C., Schmid, T., & van Wesemael, B. (2019). Imaging Spectroscopy for Soil Mapping and Monitoring. *Surveys in Geophysics*, 40(3), 361–399. <https://doi.org/10.1007/s10712-019-09524-0>

- Chawla, N. V., Bowyer, K. W., Hall, L. O., & Kegelmeyer, W. P. (2002). SMOTE: Synthetic Minority Over-sampling Technique. *Journal of Artificial Intelligence Research*, *16*, 321–357. <https://doi.org/10.1613/jair.953>
- Chen, S., Arrouays, D., Leatitia Mulder, V., Poggio, L., Minasny, B., Roudier, P., Libohova, Z., Lagacherie, P., Shi, Z., Hannam, J., Meersmans, J., Richer-de-Forges, A. C., & Walter, C. (2022). Digital mapping of GlobalSoilMap soil properties at a broad scale: A review. *Geoderma*, *409*, 115567. <https://doi.org/10.1016/j.geoderma.2021.115567>
- Cortes, C., & Vapnik, V. (1995). Support-vector networks. *Machine Learning*, *20*(3), 273–297. <https://doi.org/10.1007/BF00994018>
- De Brogniez, D., Ballabio, C., Stevens, A., Jones, R. J. A., Montanarella, L., & Van Wesemael, B. (2015). A map of the topsoil organic carbon content of Europe generated by a generalized additive model. *European Journal of Soil Science*, *66*(1), 121–134. <https://doi.org/10.1111/ejss.12193>
- Delaney, B., Tansey, K., & Whelan, M. (2025). Satellite Remote Sensing Techniques and Limitations for Identifying Bare Soil. *Remote Sensing*, *17*(4), Article 4. <https://doi.org/10.3390/rs17040630>
- Demattê, J. A. M., Fongaro, C. T., Rizzo, R., & Safanelli, J. L. (2018). Geospatial Soil Sensing System (GEOS3): A powerful data mining procedure to retrieve soil spectral reflectance from satellite images. *Remote Sensing of Environment*, *212*, 161–175. <https://doi.org/10.1016/j.rse.2018.04.047>
- Demattê, J. A. M., Rizzo, R., Rosin, N. A., Poppiel, R. R., Novais, J. J. M., Amorim, M. T. A., Rodriguez-Albarracín, H. S., Rosas, J. T. F., Bartsch, B. dos A., Vogel, L. G., Minasny, B., Grunwald, S., Ge, Y., Ben-Dor, E., Gholizadeh, A., Gomez, C., Chabrillat, S., Francos, N., Fiantis, D., ... Shepherd, K. D. (2025). A global soil spectral grid based on space sensing. *Science of The Total Environment*, *968*, 178791. <https://doi.org/10.1016/j.scitotenv.2025.178791>
- Demattê, J. A. M., Safanelli, J. L., Poppiel, R. R., Rizzo, R., Silvero, N. E. Q., Mendes, W. de S., Bonfatti, B. R., Dotto, A. C., Salazar, D. F. U., Mello, Fellipe Alcântara de Oliveira, Da Paiva, A. F. S., Souza, A. B., Santos, N. V. dos, Maria Nascimento, C., Mello, D. C., Bellinaso, H., Gonzaga Neto, L., Amorim, M. T. A., Resende, M. E. B., ... Da Lisboa, C. J. S. (2020). Bare Earth's Surface Spectra as a Proxy for Soil Resource Monitoring. *Scientific Reports*, *10*(1), 4461. <https://doi.org/10.1038/s41598-020-61408-1>
- Destatis. (2022). *Land- und Forstwirtschaft, Fischerei—Bodenfläche nach Art der tatsächlichen Nutzung*. https://www.statistischebibliothek.de/mir/servlets/MCRFileNodeServlet/DEHeft_derivate_00071957/2030510217004.pdf

- Diek, S., Fornallaz, F., & Schaepman, M. E. (2017). Barest Pixel Composite for Agricultural Areas Using Landsat Time Series. *Remote Sensing*, 9(12), 1245. <https://doi.org/10.3390/rs9121245>
- Don, A., Schumacher, J., Scherer-Lorenzen, M., Scholten, T., & Schulze, E.-D. (2007). Spatial and vertical variation of soil carbon at two grassland sites—Implications for measuring soil carbon stocks. *Geoderma*, 141(3–4), 272–282. <https://doi.org/10.1016/j.geoderma.2007.06.003>
- Dvorakova, K., Heiden, U., Pepers, K., Staats, G., van Os, G., & van Wesemael, B. (2022). Improving soil organic carbon predictions from a Sentinel-2 soil composite by assessing surface conditions and uncertainties. *Geoderma*, 116128. <https://doi.org/10.1016/j.geoderma.2022.116128>
- Dvorakova, K., Heiden, U., & van Wesemael, B. (2021). Sentinel-2 Exposed Soil Composite for Soil Organic Carbon Prediction. *Remote Sensing*, 13(9), 1791. <https://doi.org/10.3390/rs13091791>
- Dvorakova, K., Shi, P., Limbourg, Q., & van Wesemael, B. (2020). Soil Organic Carbon Mapping from Remote Sensing: The Effect of Crop Residues. *Remote Sensing*, 12(12), 1913. <https://doi.org/10.3390/rs12121913>
- Feeney, C. J., Cosby, B. J., Robinson, D. A., Thomas, A., Emmett, B. A., & Henrys, P. (2022). Multiple soil map comparison highlights challenges for predicting topsoil organic carbon concentration at national scale. *Scientific Reports*, 12(1), 1379. <https://doi.org/10.1038/s41598-022-05476-5>
- Fisher, A., Rudin, C., & Dominici, F. (2019). *All Models are Wrong, but Many are Useful: Learning a Variable's Importance by Studying an Entire Class of Prediction Models Simultaneously*.
- Frantz, D. (2019). FORCE—Landsat + Sentinel-2 Analysis Ready Data and Beyond. *Remote Sensing*, 11(9), 1124. <https://doi.org/10.3390/rs11091124>
- Frantz, D., Haß, E., Uhl, A., Stoffels, J., & Hill, J. (2018). Improvement of the Fmask algorithm for Sentinel-2 images: Separating clouds from bright surfaces based on parallax effects. *Remote Sensing of Environment*, 215, 471–481. <https://doi.org/10.1016/j.rse.2018.04.046>
- Frantz, D., Röder, A., Stellmes, M., & Hill, J. (2016). An operational radiometric landsat preprocessing framework for large-area time series applications. *IEEE Transactions on Geoscience and Remote Sensing*, 54(7), 3928–3943. Scopus. <https://doi.org/10.1109/TGRS.2016.2530856>
- Frantz, D., Roder, A., Udelhoven, T., & Schmidt, M. (2015). Enhancing the Detectability of Clouds and Their Shadows in Multitemporal Dryland Landsat Imagery: Extending Fmask. *IEEE Geoscience and Remote Sensing Letters*, 12(6), 1242–1246. <https://doi.org/10.1109/LGRS.2015.2390673>

- Frantz, D., Stellmes, M., Roder, A., Udelhoven, T., Mader, S., & Hill, J. (2016). Improving the Spatial Resolution of Land Surface Phenology by Fusing Medium- and Coarse-Resolution Inputs. *IEEE Transactions on Geoscience and Remote Sensing*, *54*(7), 4153–4164. <https://doi.org/10.1109/TGRS.2016.2537929>
- Gitelson, A., & Merzlyak, M. N. (1994). Spectral Reflectance Changes Associated with Autumn Senescence of *Aesculus hippocastanum* L. and *Acer platanoides* L. Leaves. Spectral Features and Relation to Chlorophyll Estimation. *Journal of Plant Physiology*, *143*(3), 286–292. [https://doi.org/10.1016/S0176-1617\(11\)81633-0](https://doi.org/10.1016/S0176-1617(11)81633-0)
- Gomez, C., Vaudour, E., Féret, J.-B., de Boissieu, F., & Dharumarajan, S. (2022). Topsoil clay content mapping in croplands from Sentinel-2 data: Influence of atmospheric correction methods across a season time series. *Geoderma*, *423*, 115959. <https://doi.org/10.1016/j.geoderma.2022.115959>
- Heiden, U., d'Angelo, P., Schwind, P., Karlshöfer, P., Müller, R., Zepp, S., Wiesmeier, M., & Reinartz, P. (2022). Soil Reflectance Composites—Improved Thresholding and Performance Evaluation. *Remote Sensing*, *14*(18), 4526. <https://doi.org/10.3390/rs14184526>
- Hengl, T., Nussbaum, M., Wright, M. N., Heuvelink, G. B. M., & Gräler, B. (2018). Random forest as a generic framework for predictive modeling of spatial and spatio-temporal variables. *PeerJ*, *6*, 5518. <https://doi.org/10.7717/peerj.5518>
- Hijmans, R. J. (2025). *terra: Spatial Data Analysis*. <https://github.com/rspsatial/terra>
- Huete, A. R. (1988). A soil-adjusted vegetation index (SAVI). *Remote Sensing of Environment*, *25*(3), 295–309. [https://doi.org/10.1016/0034-4257\(88\)90106-X](https://doi.org/10.1016/0034-4257(88)90106-X)
- Lal, R. (2003). Global Potential of Soil Carbon Sequestration to Mitigate the Greenhouse Effect. *Critical Reviews in Plant Sciences*, *22*(2), 151–184. <https://doi.org/10.1080/713610854>
- Lang, M., Binder, M., Richter, J., Schratz, P., Pfisterer, F., Coors, S., Au, Q., Casalicchio, G., Kotthoff, L., & Bischl, B. (2019). mlr3: A modern object-oriented machine learning framework in R. *Journal of Open Source Software*. <https://doi.org/10.21105/joss.01903>
- Lin, L. I.-K. (1989). A Concordance Correlation Coefficient to Evaluate Reproducibility. *Biometrics*, *45*(1), 255. <https://doi.org/10.2307/2532051>
- Meyer, G. E., Hindman, T. W., & Laksmi, K. (1999). *Machine vision detection parameters for plant species identification* (G. E. Meyer & J. A. DeShazer, Eds.; pp. 327–335). <https://doi.org/10.1117/12.336896>
- Meyer, H., Reudenbach, C., Wöllauer, S., & Nauss, T. (2019). Importance of spatial predictor variable selection in machine learning applications – Moving from data reproduction to spatial prediction. *Ecological Modelling*, *411*, 108815. <https://doi.org/10.1016/j.ecolmodel.2019.108815>

- Minasny, B., Malone, B. P., McBratney, A. B., Angers, D. A., Arrouays, D., Chambers, A., Chaplot, V., Chen, Z.-S., Cheng, K., Das, B. S., Field, D. J., Gimona, A., Hedley, C. B., Hong, S. Y., Mandal, B., Marchant, B. P., Martin, M., McConkey, B. G., Mulder, V. L., ... Winowiecki, L. (2017). Soil carbon 4 per mille. *Geoderma*, 292, 59–86. <https://doi.org/10.1016/j.geoderma.2017.01.002>
- Møller, A. B., Beucher, A. M., Pouladi, N., & Greve, M. H. (2020). Oblique geographic coordinates as covariates for digital soil mapping. *SOIL*, 6(2), 269–289. <https://doi.org/10.5194/soil-6-269-2020>
- Montanarella, L., & Panagos, P. (2021). The relevance of sustainable soil management within the European Green Deal. *Land Use Policy*, 100, 104950. <https://doi.org/10.1016/j.landusepol.2020.104950>
- Montandon, L. M., & Small, E. E. (2008). The impact of soil reflectance on the quantification of the green vegetation fraction from NDVI. *Remote Sensing of Environment*, 112(4), 1835–1845. <https://doi.org/10.1016/j.rse.2007.09.007>
- Montero, D., Aybar, C., Mahecha, M. D., Martinuzzi, F., Söchting, M., & Wieneke, S. (2023). A standardized catalogue of spectral indices to advance the use of remote sensing in Earth system research. *Scientific Data*, 10(1), 197. <https://doi.org/10.1038/s41597-023-02096-0>
- Murphy, B. W. (2015). Impact of soil organic matter on soil properties—A review with emphasis on Australian soils. *Soil Research*, 53(6), 605–635. <https://doi.org/10.1071/SR14246>
- Nguyen, C. T., Chidthaisong, A., Kieu Diem, P., & Huo, L.-Z. (2021). A Modified Bare Soil Index to Identify Bare Land Features during Agricultural Fallow-Period in Southeast Asia Using Landsat 8. *Land*, 10(3), 231. <https://doi.org/10.3390/land10030231>
- Paustian, K., Collier, S., Baldock, J., Burgess, R., Creque, J., DeLonge, M., Dungait, J., Ellert, B., Frank, S., Goddard, T., Govaerts, B., Grundy, M., Henning, M., Izaurralde, R. C., Madaras, M., McConkey, B., Porzig, E., Rice, C., Searle, R., ... Jahn, M. (2019). Quantifying carbon for agricultural soil management: From the current status toward a global soil information system. *Carbon Management*, 10(6), 567–587. <https://doi.org/10.1080/17583004.2019.1633231>
- Poeplau, C., Don, A., Flessa, H., Heidkamp, A., Jacobs, A., & Prietz, R. (2020). Erste Bodenzustandserhebung Landwirtschaft – Kerndatensatz. *OpenAgrar*. <https://doi.org/10.3220/DATA20200203151139>
- Poeplau, C., Jacobs, A., Don, A., Vos, C., Schneider, F., Wittnebel, M., Tiemeyer, B., Heidkamp, A., Prietz, R., & Flessa, H. (2020). Stocks of organic carbon in German agricultural soils—Key results of the first comprehensive inventory. *Journal of Plant Nutrition and Soil Science*, 183(6), 665–681. <https://doi.org/10.1002/jpln.202000113>

- Poeplau, C., Prietz, R., & Don, A. (2022). Plot-scale variability of organic carbon in temperate agricultural soils—Implications for soil monitoring. *Journal of Plant Nutrition and Soil Science*, 185(3), 403–416. <https://doi.org/10.1002/jpln.202100393>
- Poeplau, C., Vos, C., & Don, A. (2017). Soil organic carbon stocks are systematically overestimated by misuse of the parameters bulk density and rock fragment content. *SOIL*, 3(1), 61–66. <https://doi.org/10.5194/soil-3-61-2017>
- Prout, J. M., Shepherd, K. D., McGrath, S. P., Kirk, G. J. D., & Haefele, S. M. (2021). What is a good level of soil organic matter? An index based on organic carbon to clay ratio. *European Journal of Soil Science*, 72(6), 2493–2503. <https://doi.org/10.1111/ejss.13012>
- R Core Team. (2022). *R: A Language and Environment for Statistical Computing*. R Foundation for Statistical Computing. <https://www.R-project.org/>
- Rasmussen, C., Heckman, K., Wieder, W. R., Keiluweit, M., Lawrence, C. R., Berhe, A. A., Blankinship, J. C., Crow, S. E., Druhan, J. L., Hicks Pries, C. E., Marin-Spiotta, E., Plante, A. F., Schädel, C., Schimel, J. P., Sierra, C. A., Thompson, A., & Wagai, R. (2018). Beyond clay: Towards an improved set of variables for predicting soil organic matter content. *Biogeochemistry*, 137(3), 297–306. <https://doi.org/10.1007/s10533-018-0424-3>
- Rau, K., Eggenberger, K., Schneider, F., Hennig, P., & Scholten, T. (2024). How can we quantify, explain, and apply the uncertainty of complex soil maps predicted with neural networks? *Science of The Total Environment*, 944, 173720. <https://doi.org/10.1016/j.scitotenv.2024.173720>
- Rawlins, B. G., Marchant, B. P., Smyth, D., Scheib, C., Lark, R. M., & Jordan, C. (2009). Airborne radiometric survey data and a DTM as covariates for regional scale mapping of soil organic carbon across Northern Ireland. *European Journal of Soil Science*, 60(1), 44–54. <https://doi.org/10.1111/j.1365-2389.2008.01092.x>
- Rogge, D., Bauer, A., Zeidler, J., Mueller, A., Esch, T., & Heiden, U. (2018). Building an exposed soil composite processor (SCMaP) for mapping spatial and temporal characteristics of soils with Landsat imagery (1984–2014). *Remote Sensing of Environment*, 205, 1–17. <https://doi.org/10.1016/j.rse.2017.11.004>
- Rufin, P., Frantz, D., Yan, L., & Hostert, P. (2021). Operational Coregistration of the Sentinel-2A/B Image Archive Using Multitemporal Landsat Spectral Averages. *IEEE Geoscience and Remote Sensing Letters*, 18(4), 712–716. <https://doi.org/10.1109/LGRS.2020.2982245>
- Safanelli, J. L., Chabrillat, S., Ben-Dor, E., & Demattê, J. A. M. (2020). Multispectral Models from Bare Soil Composites for Mapping Topsoil Properties over Europe. *Remote Sensing*, 12(9), 1369. <https://doi.org/10.3390/rs12091369>

- Shabou, M., Mougenot, B., Chabaane, Z. L., Walter, C., Boulet, G., Aissa, N. B., & Zribi, M. (2015). Soil Clay Content Mapping Using a Time Series of Landsat TM Data in Semi-Arid Lands. *Remote Sensing*, 7(5), Article 5. <https://doi.org/10.3390/rs70506059>
- Sharififar, A., Sarmadian, F., Malone, B. P., & Minasny, B. (2019). Addressing the issue of digital mapping of soil classes with imbalanced class observations. *Geoderma*, 350, 84–92. <https://doi.org/10.1016/j.geoderma.2019.05.016>
- Silvero, N. E. Q., Demattê, J. A. M., Amorim, M. T. A., Santos, N. V. dos, Rizzo, R., Safanelli, J. L., Poppiel, R. R., Mendes, W. de S., & Bonfatti, B. R. (2021). Soil variability and quantification based on Sentinel-2 and Landsat-8 bare soil images: A comparison. *Remote Sensing of Environment*, 252, 112117. <https://doi.org/10.1016/j.rse.2020.112117>
- Stenberg, B. (2010). Effects of soil sample pretreatments and standardised rewetting as interacted with sand classes on Vis-NIR predictions of clay and soil organic carbon. *Geoderma*, 158(1), 15–22. <https://doi.org/10.1016/j.geoderma.2010.04.008>
- Stumpf, F., Behrens, T., Schmidt, K., & Keller, A. (2024). Exploiting Soil and Remote Sensing Data Archives for 3D Mapping of Multiple Soil Properties at the Swiss National Scale. *Remote Sensing*, 16(15), Article 15. <https://doi.org/10.3390/rs16152712>
- Sulik, J. J., & Long, D. S. (2016). Spectral considerations for modeling yield of canola. *Remote Sensing of Environment*, 184, 161–174. <https://doi.org/10.1016/j.rse.2016.06.016>
- Thünen-Institut. (2022). *Forstliche Großlandschaften* (2011). https://atlas.thuenen.de/layers/wgwb:geonode:wgwb_forstl_gl_2011
- Tucker, C. J. (1979). Red and photographic infrared linear combinations for monitoring vegetation. *Remote Sensing of Environment*, 8(2), 127–150. [https://doi.org/10.1016/0034-4257\(79\)90013-0](https://doi.org/10.1016/0034-4257(79)90013-0)
- Tziolas, N., Tsakiridis, N., Chabrilat, S., Demattê, J. A. M., Ben-Dor, E., Gholizadeh, A., Zalidis, G., & van Wesemael, B. (2021). Earth Observation Data-Driven Cropland Soil Monitoring: A Review. *Remote Sensing*, 13(21), 4439. <https://doi.org/10.3390/rs13214439>
- Urbina-Salazar, D., Vaudour, E., Richer-de-Forges, A. C., Chen, S., Martelet, G., Baghdadi, N., & Arrouays, D. (2023). Sentinel-2 and Sentinel-1 Bare Soil Temporal Mosaics of 6-year Periods for Soil Organic Carbon Content Mapping in Central France. *Remote Sensing*, 15(9), 2410. <https://doi.org/10.3390/rs15092410>
- Van Deventer, A. P., Ward, A. D., Gowda, P. M., & Lyon, J. G. (1997). Using thematic mapper data to identify contrasting soil plains and tillage practices. *Photogrammetric Engineering and Remote Sensing*, 63(1), 87–93. Scopus.
- Vaserstein, L. N. (1969). Markov processes over denumerable products of spaces, describing large systems of automata. *Problemy Peredachi Informatsii*, 64–72.

- Vaudour, E., Gholizadeh, A., Castaldi, F., Saberioon, M., Borůvka, L., Urbina-Salazar, D., Fouad, Y., Arrouays, D., Richer-de-Forges, A. C., Biney, J., Wetterlind, J., & van Wesemael, B. (2022). Satellite Imagery to Map Topsoil Organic Carbon Content over Cultivated Areas: An Overview. *Remote Sensing*, *14*(12), 2917. <https://doi.org/10.3390/rs14122917>
- Vaudour, E., Gomez, C., Lagacherie, P., Loiseau, T., Baghdadi, N., Urbina-Salazar, D., Loubet, B., & Arrouays, D. (2021). Temporal mosaicking approaches of Sentinel-2 images for extending topsoil organic carbon content mapping in croplands. *International Journal of Applied Earth Observation and Geoinformation*, *96*, 102277. <https://doi.org/10.1016/j.jag.2020.102277>
- Wang, F., Huang, J., Tang, Y., & Wang, X. (2007). New Vegetation Index and Its Application in Estimating Leaf Area Index of Rice. *Rice Science*, *14*(3), 195–203. [https://doi.org/10.1016/S1672-6308\(07\)60027-4](https://doi.org/10.1016/S1672-6308(07)60027-4)
- Wetterlind, J., Simmler, M., Castaldi, F., Borůvka, L., Gabriel, J. L., Gomes, L. C., Khosravi, V., Kıvrak, C., Koparan, M. H., Lázaro-López, A., Łopatka, A., Liebisch, F., Rodriguez, J. A., Savaş, A. Ö., Stenberg, B., Tunçay, T., Vinci, I., Volungevičius, J., Žydelis, R., & Vaudour, E. (2025). Influence of Soil Texture on the Estimation of Soil Organic Carbon From Sentinel-2 Temporal Mosaics at 34 European Sites. *European Journal of Soil Science*, *76*(1), e70054. <https://doi.org/10.1111/ejss.70054>
- Wiesmeier, M., Urbanski, L., Hobbey, E., Lang, B., von Lützwow, M., Marin-Spiotta, E., van Wesemael, B., Rabot, E., Ließ, M., Garcia-Franco, N., Wollschläger, U., Vogel, H.-J., & Kögel-Knabner, I. (2019). Soil organic carbon storage as a key function of soils—A review of drivers and indicators at various scales. *Geoderma*, *333*, 149–162. <https://doi.org/10.1016/j.geoderma.2018.07.026>
- Zepp, S., Heiden, U., Bachmann, M., Wiesmeier, M., Steininger, M., & van Wesemael, B. (2021). Estimation of Soil Organic Carbon Contents in Croplands of Bavaria from SCMaP Soil Reflectance Composites. *Remote Sensing*, *13*(16), 3141. <https://doi.org/10.3390/rs13163141>
- Zhu, Z., & Woodcock, C. E. (2012). Object-based cloud and cloud shadow detection in Landsat imagery. *Remote Sensing of Environment*, *118*, 83–94. <https://doi.org/10.1016/j.rse.2011.10.028>
- Žížala, D., Minařík, R., Skála, J., Beitlerová, H., Juřicová, A., Reyes Rojas, J., Penížek, V., & Zádorová, T. (2022). High-resolution agriculture soil property maps from digital soil mapping methods, Czech Republic. *CATENA*, *212*, 106024. <https://doi.org/10.1016/j.catena.2022.106024>